IEEE Access
Multidisciplinary | Rapid Review | Open Access Journal

Received 22 May 2023, accepted 4 June 2023, date of publication 8 June 2023, date of current version 15 June 2023.

Digital Object Identifier 10.1109/ACCESS.2023.3284311

RESEARCH ARTICLE

Optimizing the Operation and Coordination of Multi-Carrier Energy Systems in Smart Microgrids Using a Stochastic Approach

GHADA ABDULNASSER[1], ABDELFATAH ALI[1,2], MOSTAFA F. SHAABAN[2], (Senior Member, IEEE), AND ESSAM E. M. MOHAMED[1]

[1]Department of Electrical Engineering, South Valley University, Qena 83523, Egypt
[2]Department of Electrical Engineering, American University of Sharjah, Sharjah, United Arab Emirates

Corresponding author: Abdelfatah Ali (abdelfatahm@aus.edu)

This work was supported in part by the American University of Sharjah under Grant FRG22-C-E24, and in part by the Open Access Program from the American University of Sharjah.

ABSTRACT Energy hubs (EHs) have become essential to facilitate the coupling of the various energy carriers in smart microgrids characterized by high penetration levels of various renewable energy sources (RES), such as photovoltaics and wind power. Optimal operation and coordination of these microgrid resources are crucial for satisfying electrical and thermal demands with minimal cost and achieving eco-friendly operation. To this end, this paper proposes a stochastic multi-objective optimization approach for optimal operation and coordination of RES, EH systems, and plug-in electric vehicles (PEVs). The EH includes compressed air energy storage, battery energy storage, and thermal energy storage. The objective functions to be minimized are operating costs and emissions. The proposed approach considers the uncertainties of RES, electrical and thermal demands, electrical prices during seasonal-based horizons, the stochastic nature of PEV's owners' driving habits, and various microgrid operational constraints. Furthermore, a price-based demand response program is employed considering the end-user's discomfort. The multi-objective grey wolf optimizer is employed to solve the proposed optimization problem and obtain the Pareto-optimal solutions. Different case studies are performed to demonstrate the proposed approach's effectiveness. The simulation results show that the proposed approach can reduce the operation cost and emissions by 64.1% and 57.6%, respectively.

INDEX TERMS Multi-carrier systems, energy hubs, compressed air energy storage, plug-in electric vehicle, renewable energy sources.

NOMENCLATURE

ABBREVIATIONS

BESS	Battery energy storage.
CAES	Compressed air energy storage.
CHP	Combined heat and power.
DSMP	Demand side management programs.
EH	Energy hub.
EHO	Energy hub operator.
MCES	Multi-carrier energy system.
MOGWO	Multi-objective grey wolf optimizer.
PEV	Plug-in electric vehicles.
PV	Photovoltaics system.
RES	Renewable energy sources.
SOC	State of charge.
TES	Thermal energy storage.
WT	Wind turbines.

INDICES AND SETS

j	Index of PEV.
n	Index of EH.
t	Index of time.
s	Index of scenario.
N_{OBJ}	Total number of objectives.
N_{PF}	Total number of Pareto front solutions.

The associate editor coordinating the review of this manuscript and approving it for publication was Xiaodong Liang.

PARAMETERS

AMR_j	All-electric range for the j th PEV.
C_{AIR}	Specific heat of the air.
$C_{batt,j}$	Battery capacity of the j th PEV.
CR	Power rate limit of the BESS in kW.
$Distance_j$	traveling distance for the j th PEV.
$E^{TES}_{min}/E^{TES}_{max}$	Min/ Max heat energy limits of the TES.
$E_{con/mile,j}$	Energy consumption per mileage of the j th PEV.
$E^{PEV}_{min}/E^{PEV}_{max}$	Min/Max energy limit of the PEV's battery.
γ^{NG}	Natural gas price in \$/Gj.
$\gamma^{Ch}_{BESS}/\gamma^{Dis}_{BESS}$	Charging and discharging efficiency of the BESS.
$\gamma^{Ch}_{PEV}/\gamma^{Dis}_{PEV}$	Charging and discharging efficiencies of the PEV.
$\gamma^{CO_2}_{Net}/\gamma^{NO_x}_{Net}/\gamma^{SO_x}_{Net}$	Emission factor of the grid in g/kWh.
$\gamma^{CO_2}_{c}/\gamma^{NO_x}_{c}/\gamma^{SO_x}_{c}$	Emission factors of the CAES in g/Gj.
γGrid	Electricity market price in \$/kWh.
σ_{Ar}/μ_{Ar}	Mean and standard deviation for the arrival time of the PEV.
EC_{min}/EC_{max}	Min/Max energy content of the CAES in kWh.
Er	Energy ratio of the CAES in kWh.
$Mr^{ele,Down}/Mr^{ele,Up}$	Max down/up electric power ratios transferred.
OM^{c}	Variable operation and maintenance cost of the CAES in charging and simple cycle modes in \$/kWh.
OM^{exp}	Variable operation and maintenance cost of the CAES in discharging mode in \$/kWh.
PC^{EXP}_{max}	Min/Max and simple cycle power of the CAES in kW.
$P^{TES,in}_{max}/P^{TES,DR}_{max}$	Max heat power injection and drawing limits of the TES.
$\pi^{ele,Down}_{DRP}/\pi^{ele,Up}_{DRP}$	Ascending and descending costs of electric DRP
$SOC^{BESS}_{min}/SOC^{BESS}_{max}$	Min/Max SOC limits of the BESS.
$SOC^{PEV}_{min}/SOC^{PEV}_{max}$	Min/Max SOC limits of the PEV.
T^{CW}	Temperature of cold water.
$T^{WS}_{min}/T^{WS}_{max}$	Min/Max hot water temperature limits for customer satisfaction.
$T^{indoor}_{min}/T^{indoor}_{max}$	Min/Max indoor air temperature limits for customer satisfaction.
V^{ws}	Volume of hot water storage.
$P^{TES,in}_{max}/P^{TES,DR}_{max}$	Max heat power injection and drawing limits of the TES.
$\pi^{ele,Down}_{DRP}/\pi^{ele,Up}_{DRP}$	Ascending and descending costs of electric DRP.
R	Heat resistance of the walls.
$SOC^{BESS}_{min}/SOC^{BESS}_{max}$	Min/Max SOC limits of the BESS.

VARIABLES

$Demand_{s,t,n}$	Electrical demand of the *nth* EH.
$E^{PEV}_{s,t,j}$	Electrical energy content of the PEV's battery in kWh.
$E^{TES}_{s,t,n}$	Thermal energy content of the TES in kWh.
$EC_{s,t,n}$	Electrical energy content of the CAES in kWh.
$H^{WS}_{s,t,n}$	Thermal energy transferred to the hot water storage.
$H^{AIR}_{t,s}$	Thermal energy transferred into household.
$OC^{CAES}_{s,t,n}$	Operation cost of the CAES.
$PB^{Ch}_{s,t,n}/PB^{Dis}_{s,t,n}$	Charging/discharging power of the BESS in kW.
$PB^{Ch,PEV}_{s,t,j}/PB^{Dis,PEV}_{s,t,j}$	Charging/discharging power of the PEV in kW.
$PC^{Ch}_{s,t,n}/PC^{Dis}_{s,t,n}$	Charging/discharging power of the CAES in kW.
$PC^{Sim}_{s,t,n}$	Simple cycle power of the CAES in kW.
$PGrid_{s,t,n}$	Power transaction of the *nth* EH with utility grid.
$P_{LOT,t,s}$	Parking lot power in kW.
$P^{ele,Down}_{t,s}/P^{ele,Up}_{t,s}$	Electric power descended and ascended by DRP in kW.
$SOC^{BESS}_{s,t,n}$	State of charge of the BESS.
$SOC^{PEV}_{s,t,j}$	State of charge of the PEV.
$T^{WS}_{s,t,n}$	Water temperature at t.
$T^{indoor}_{t,s}/T^{outdoor}_{t,s}$	Indoor/outdoor household's temperature.
$V^{COLD}_{s,t,n}$	Volume of the cold water entering the tank.

BINARY VARIABLES

$uc^{Ch}_{s,t,n}/uc^{Dis}_{s,t,n}/uc^{Sim}_{s,t,n}$	Charging, discharging, and simple cycle states of the CAES.
$b^{Ch}_{s,t,n}/b^{Dis}_{s,t,n}$	Charging and discharging binary variables of the BESS.
$I^{Ch,PEV}_{s,t,j}/I^{Dis,PEV}_{s,t,j}$	Charging and discharging binary variables of the PEV.
$I^{ele,Down}_{t,s}/I^{ele,Up}_{t,s}$	Decrement and increment status of electric demand.

I. INTRODUCTION

Nowadays, the multi-carrier system has attracted significant attention globally [1], [2]. Compared to traditional decoupled energy systems, a multi-carrier energy system (MCES) presents a flexible, reliable, and efficient approach for the coordination of different energy resources [3], [4], [5]. In this regard, the energy hub (EH) concept basically interfaces

networked streamlines for various energy infrastructures such as electricity, natural gas, and heat which are required to satisfy consumers' demands [6]. When connected to the distribution system, EH can facilitate the local co-generation, tri-generation, transfer, and distribution of different energy forms [7]. Furthermore, an EH employs a diverse variety of technologies, including renewable energy sources (RES), combined heat and power (CHP), plug-in electric vehicles (PEV), compressed air energy storage (CAES), and battery energy storage systems (BESS).

So far, numerous studies have investigated the optimal scheduling and management of various energy resources integrated into the multi-carrier EH-based microgrids. In this regard, authors of [3] have investigated a two-level optimization scheme for optimal day-ahead scheduling of an active distribution system integrating multiple EHs. In addition, [8], [9] have proposed MCES management to participate in the energy market and present a model of a smart city. Moreover, optimal day-ahead scheduling of a networked multi-carrier energy microgrid system is proposed in [10], including CHP units, gas-fired boilers, power-to-gas units (P2G), electrical and thermal storage, and electrical heat pumps, which shows the flexible day-ahead operation of the networked multi-carrier energy microgrid system.

Regarding the fossil energy crisis and global warming, global agreements have been set to move towards cleaner resources [11], [12]. Consequently, RES has been employed extensively across the globe, providing a cleaner, sustainable, and more stable environment for the survival of human beings. Accordingly, authors in [13], and [14] have addressed the minimization of CO2 as an objective with the integration of RES to contribute to CO2 reduction. Yet, the optimal scheduling and management of the RES (e.g., photovoltaics (PV) and wind turbines (WT)) can be quite challenging due to uncertainty associated with the natural resources, e.g., solar radiation and wind speed. For instance, a comprehensive multi-carrier microgrid scheme is established in [15] to boost system flexibility and compensate for the volatility nature of the RESs. The unstable nature of the demands and prices has also been considered by utilizing the probabilistic load flow approach.

Generally, Compressed air energy storage (CAES) is presented as a mechanical energy storage technology for storing electrical energy [16]. Typically, CAES could play a vital role in providing some ancillary services in the network, such as load leveling, peak shaving, time shifting, energy management, and enhancing power quality in case of the high penetration level of RES [17]. Therefore, an optimal operation schedule is considered in [18], based on integrating a CAES for storing electrical energy and considering uncertainty associated with the RES generation, electrical, thermal, and freshwater demands. Nevertheless, waste heat is generated during the discharge process, which could lead to severe heat pollution, exacerbate the greenhouse crisis, and lead to more thermal issues. As a remedy, the authors in [19] have introduced a waste heat recovery system that explicitly utilizes waste heat recovery cycles, e.g., Rankine and Kalina cycles leading to an increase in the production capacity up to 2.47% and an improvement in energy round trip efficiency by 1.69–2.67% compared to stand-alone CAES plants.

Furthermore, electrochemical energy storage, such as BESS, has also been proven to provide stability and security for the distribution network operation by ensuring the balance between the intermittent generation of RES and the demands [20]. Moreover, BESS is vital in minimizing the cost of imported grid energy and maximizing profit [21]. Compared to CAES, BESS does not generate harmful emissions during the charge and discharge cycles leading to cleaner operation. Nevertheless, it will eventually produce hazardous waste making its disposal an extremely challenging task [22]. Typically, a stochastic model investigation of the optimal operation of the EH was addressed in [23]. The objective was to minimize the total energy costs, including different energy conversion and storage devices.

Along with the undesirable emissions generated by conventional electrical distributed generators, harmful emissions are massively produced due to the operation of the internal computation engine vehicles [24]. Accordingly, global regulations have been set calling for alternatives, resulting in PEV being at the top of the list [25]. Not only that PEV contribute to a de-carbonized operation, but it also provides aggregation for electrical energy storage. Accordingly, The authors of [26] have proposed the optimal operation of the EH by integrating RES, plug-in hybrid electric vehicles (PHEV), fuel cells, and hydrogen storage units. The authors have suggested using the information gap decision theory (IGDT) to model the uncertainty posed by the PHEV.

One vital aspect of obtaining a reliable microgrid operation is to have a controlled-based demand. Therefore, consumers' cooperation with the energy hub operator (EHO) in terms of changing their consumption patterns according to typical demand side management programs (DSMP) would provide a stable and reliable operation for the microgrid [27]. This alteration in consumption patterns could be according to price or incentive-based programs [28]. An integral aspect of DSMPs termed as demand response program (DRP) concept is well-established and widely deployed to EHs. Therefore, various research works have been addressed to clarify the role of DRP deployment in EHs. For instance, [29] has introduced the bender decomposition approach to solve a complex model of stochastic operation and planning of EHs, considering DRPs.

Industrial, residential, and commercial EHs were proposed in [30] to investigate the influence of coordinated and uncoordinated power transactions on power loss, operation cost, and emission. Here, the AC optimal power flow was implemented to avoid any unauthorized power transfers in the system. Moreover, an integrated energy hub system as part of the electrical system is modeled. A bi-level optimization framework was established to obtain a cost-effective operation, considering the uncertainties of wind speed, electrical demands, and real-time prices. In [32], the optimal power and gas flow was investigated. The objective was to minimize the operation

TABLE 1. A comparison among literature related to energy hub-based microgrids.

Ref	Generation resources	Storages	Objectives		Uncertainty				V2G	DRP	Scheduling model
			Cost	Emission	Price	Demand	RES	PEV			
[1]	CHP, PV, WT	PEV, TES	✓	✗	✓	✓	✓	✓	✗	✗	Stochastic Day-ahead
[6]	CHP, PV, WT	TES	✓	✗	✓	✓	✓	✗	✗	✓	Stochastic Day-ahead
[10]	CHP	BESS, TES	✓	✗	✗	✗	✗	✗	✗	✗	Deterministic Day-ahead
[13]	CHP, PV, WT	BESS, TES	✓	CO_2	✗	✓	✓	✗	✗	✗	Stochastic Day-ahead
[17]	WT	CAES	✓	✗	✓	✓	✓	✗	✗	✗	Stochastic Day-ahead
[25]	PV, WT, P2H	Hydrogen storage, TES, PHEV	✓	✗	✓	✓	✓	✓	✗	✗	Stochastic Day-ahead
[33]	PV, WT	BESS, CAES, PEV, TES	✓	CO_2, NO_x, So_x	✗	✓	✓	✓	✗	✓	Robust Day-ahead
Pro.	PV, WT	BESS, CAES, PEV, TES	✓	CO_2, NO_x, So_x	✓	✓	✓	✓	✓	✓	Stochastic Seasonal approach

costs of electric and gas, in consequence, the proposed model has accounted for a 4% total reduction in the operation cost.

As the literature review reveals, a comprehensive multi-objective scheduling framework addressing the EH-based microgrid has not been fully established. Most of the published literary work has ignored the simultaneous joint operation of the CAES along with the BESS, PEV, and TES to achieve an economic operation and eco-friendly process. Moreover, as the seasons change, solar irradiance, wind speed, and the pattern of the end-users' electrical and thermal demands change accordingly. Thus, the comprehensive scheduling scheme should consider the seasonal scheduling horizon. The effect of the stochastic nature associated with the RES, demand, price, and PEV has also been neglected in most of the literature reviewed. Moreover, the effect of the DRP must be emphasized.

This paper proposes a stochastic multi-objective mixed-integer nonlinear programming (MINLP) optimization approach for optimizing the operation and coordination of RES, EH systems, and PEVs to minimize operational costs and emissions. A hybrid CAES and BESS-based-EHs interconnected to microgrids are considered. Moreover, thermal demand satisfaction is handled utilizing the thermal discharge of the CAES along with TES. The model also includes the DRP that considers the discomfort cost of end-users. Furthermore, the study investigates the impact of the presence of PEV parking lots at various locations and the uncertainties associated with RES, different load demands, and electricity prices. The multi-objective grey wolf (MOGWO) optimizer is employed to solve the proposed optimization problem and obtain the Pareto-optimal solutions. The main contribution of this work is summarized in Table 1 and can be concisely stated as follows:

- Proposing a stochastic multi-objective MINLP optimization framework considering the uncertainty associated with RES, distance traveled, arrival time, and the initial state of charge of PEVs, besides thermal and electrical demands and electricity market prices.
- Developing a hybrid coordinated operation model consisting of CAES and BESS based-EHs along with TES for satisfying electrical and thermal demand.
- Considering multiple parking lots connected to the microgrid to analyze the influence of the coordinated seasonal charging/discharging of the PEVs which would serve as a moveable storage system to improve the sustainability and flexibility of the system.
- Analyzing the impact of DRP on the total operation cost. Consequently, the end-users would be confronted with a degree of discomfort. In this regard, the minimization of an end-users discomfort cost is addressed.

This paper is organized as follows; the system description is established in section II. Afterward, a mathematical formulation is carried out in section III. The uncertainty modeling is introduced in section IV, while electrical and thermal power equilibrium equations are set in section V. The solution algorithm is explained in section VI. The case studies and simulation results are introduced in sections VII and VIII, respectively. Eventually, the study conclusions are organized in section IX.

II. SYSTEM DESCRIPTION

In this section, the proposed model regarding the optimal scheduling and management of multiple EHs incorporated

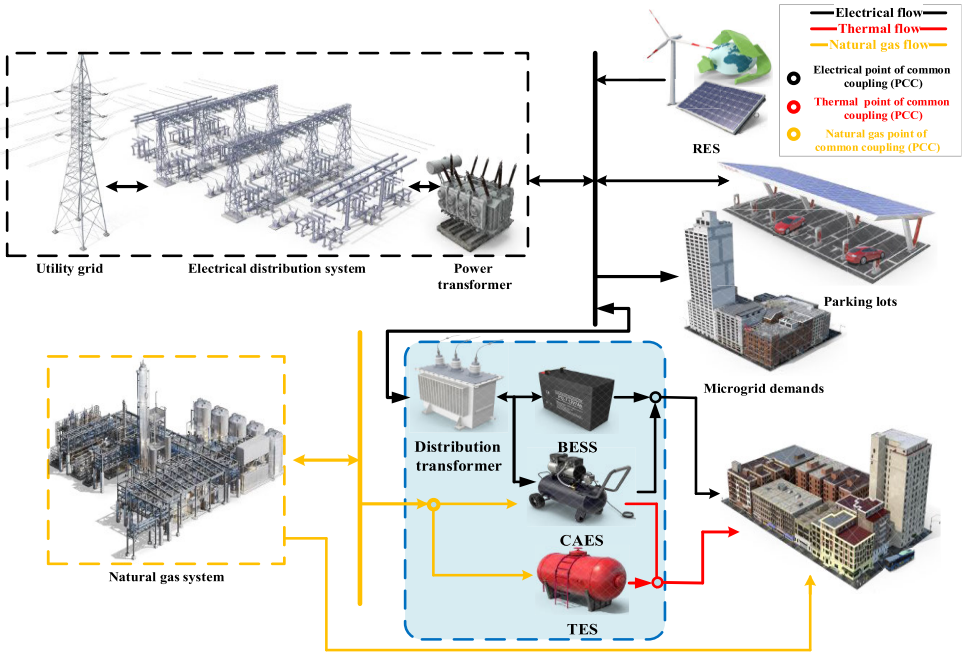

FIGURE 1. The basic construction of the proposed EHs-based system.

into the distribution system is fully developed, as depicted in Figs. 1 and 2. Firstly, Fig. 1 represents a comprehensive overview of the proposed multi-carrier system, which consists of an electrical distribution system and a natural gas network. The energy sources are the incoming electricity and natural gas; meanwhile, the consumption consists of electricity and thermal infrastructures. The energy exchange among different energy equipment takes place at various points marked as a point of common coupling (PCC), that is, the electrical PCC, the natural gas PCC, and the thermal PCC. Typically, the electrical system consists of the utility grid, RESs, parking lots, EHs, and demands located at various bus locations.

Mainly, the electric distribution system used in this study consists of a typical IEEE-33 radial distribution system. Moreover, the distribution network incorporates two types of non-dispatchable generations located at suggested locations according to the investors' preferences for particular locations and space availability. Alternatively, other technical suggestions to allocate these resources would consider making them planning decision variables in the optimization algorithm. As evident from Fig. 2, three PV systems are located on buses 19, 23, and 27. Additionally, three WT farms are located on 14, 16, and 31. Furthermore, the proposed model implements four EHs at suggested electric buses 8, 13, 16, and 33. Generally, and as illustrated in Fig. 1, each EH is equipped with CAES, BESS, TES, and thermal demands besides controllable-based electric demands, which could be controlled in response to a controlling signal from the EHO.

It is noteworthy that each EH at each bus has the same configuration, though these configurations could differ according to the specific case study under consideration. In case of any deficiency in the demand satisfaction process, each EH could purchase energy from the upstream grid. On the contrary, whenever experiencing a surplus generation EH could sell this power leading to a power transaction with the upstream grid in either direction. As an electrical energy, storage aggregator, four parking lots were plugged into buses 5, 12, 19, and 28. The optimal scheduled charging and discharging of the PEV could mitigate operational costs and emissions.

III. MATHEMATICAL FORMULATION

A. OBJECTIVE FUNCTIONS

The suggested model addresses the minimization of two objectives, as in (1). The proposed stochastic model is an expected value-based model that is developed to handle uncertain parameters. Each function is then evaluated and weighted according to the probability obtained, as depicted in (2).

$$\min_{\theta}(f_1, f_2) \tag{1}$$

$$f_{\mathrm{EXP}} = \sum_{t\in T}\sum_{s\in S} f(t,s) \times \rho(t,s) \tag{2}$$

Here, f_1 and f_2 represent the cost and emission objectives, respectively; θ represents the vector of the decision variables, which includes the charging power of the *nth* CAES at scenario sand time t($PC^{Ch}_{s,t,n}$), the discharging power of the CAES ($PC^{Dis}_{s,t,n}$), the simple cycle power of the CAES ($PC^{Sim}_{s,t,n}$), the charging power of the BESS attand scenario s at the *nth* EH ($PB^{Ch}_{s,t,n}$), the discharging power of the BESS ($PB^{Dis}_{s,t,n}$), and the parking lot power ($P_{LOT,t,s}$) all in kW; f_{EXP} denotes the expected value obtained for objective function f (t, s) for each

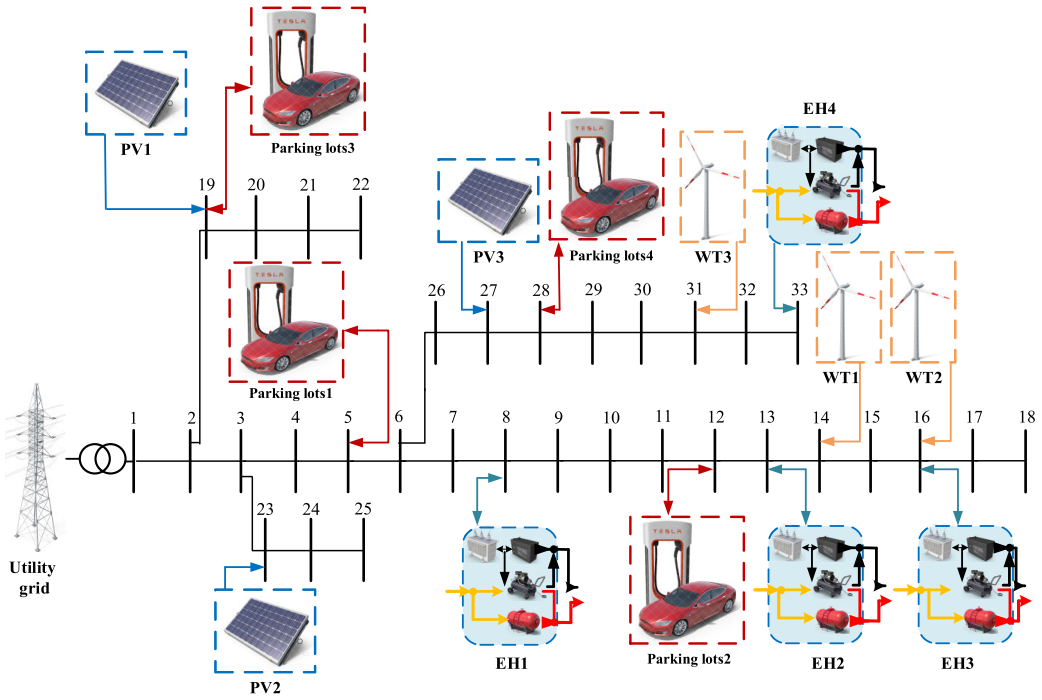

FIGURE 2. Scheme of the proposed IEEE-33 bus system with multiple EHs and RES.

time segment tand scenario s; The probability obtained for specific t and s is denoted by $\rho\,(t, s)$.

Initially, the total operation cost for multiple EHs is represented by (3), which includes the operation cost of *n*th CAES at time t and scenario s represented as $OC^{\text{CAES}}_{s,t,n}$. Moreover, the power transaction of the *nth* EH with the upstream grid for a specific electricity market price in kWh is defined as $\text{PGrid}_{s,t,n}$ and γGrid , respectively. The implementation cost of the electric DRP, considering the discomfort experienced by the participants, is represented by C_{eleDR}.

$$f_1 = \sum_{s=1}^{S} \rho_s \left(\sum_{t=1}^{T} \sum_{n=1}^{N} \left\{ \text{OC}^{\text{CAES}}_{s,t,n} + \text{PGrid}_{s,t,n} \times \gamma\text{Grid} \right\} + C_{\text{eleDR}} \right) \tag{3}$$

$$f_2 = \sum_{s=1}^{S} \rho_s \left(\sum_{t=1}^{T} \sum_{n=1}^{N} \{ \text{PGrid}_{s,t,n} \times \left(\gamma^{\text{CO}_2}_{\text{Net}} + \gamma^{\text{NO}_x}_{\text{Net}} + \gamma^{\text{SO}_x}_{\text{Net}} \right) + (\text{PC}^{\text{Dis}}_{s,t,n} \times \text{HR}^{\text{Dis}} + \text{PC}^{\text{Sim}}_{s,t,n} \times \text{HR}^{\text{Sim}}) \times (\gamma^{\text{CO}_2}_{c} + \gamma^{\text{NO}_x}_{c} + \gamma^{\text{SO}_x}_{c}) \} \right) \tag{4}$$

The emission diffused due to burning natural gas in the CAES plants and equipment owned by the upstream grid is established in (4). The terms $\gamma^{\text{CO}_2}_{\text{Net}}$, $\gamma^{\text{NO}_x}_{\text{Net}}$, and $\gamma^{\text{SO}_x}_{\text{Net}}$ represent the emission factor of the grid in g/kWh. Furthermore, HR^{Dis} and HR^{Sim} represent the CAES heat rate in discharging and simple cycle modes in Gj/kWh, respectively. Finally, the terms $\gamma^{\text{CO}_2}_{c}$, $\gamma^{\text{NO}_x}_{c}$, and $\gamma^{\text{SO}_x}_{c}$ indicate emission factors of the CAES in g/kWh.

B. COMPRESSED AIR ENERGY STORAGE MODEL

To realize the economic operation management of the *nth* CAES for each scenario and time segment, the CAES operation cost is considered as follows:

$$\begin{aligned} \text{OC}^{\text{CAES}}_{s,t,n} = & \left[\text{PC}^{\text{Dis}}_{s,t,n} \times \left(\text{HR}^{\text{Dis}} \times \gamma^{\text{NG}} + \text{OM}^{\text{exp}} \right) \right] \\ & + \left[\text{PC}^{\text{Sim}}_{s,t,n} \times \left(\text{HR}^{\text{Sim}} \times \gamma^{\text{NG}} + \text{OM}^{c} \right) \right] \\ & + \left[\text{PC}^{\text{Ch}}_{s,t,n} \times \text{OM}^{c} \right] \qquad \forall\, s, t, n \end{aligned} \tag{5}$$

Generally, CAES could operate in three modes: charging, discharging, and simple cycle modes [33]. For discharging variable and operation costs, the first term is established. The parameters γ^{NG} and OM^{exp} define the natural gas price (\$/Gj) and variable operation and maintenance cost of the CAES in discharging mode (\$/kWh), respectively. Similarly, the second and third terms of (5) declare simple cycle and charging costs. The parameter OM^{c} represents the variable operation and maintenance cost of the CAES in charging and simple cycle modes (\$/kWh).

It is essential to restrict the operation of CAES to some technical constraints, which are stated in (6) to (13). It is worth mentioning that CAES cannot operate in different modes simultaneously; this is denoted by (6), where $\text{uc}^{\text{Ch}}_{s,t,n}$, $\text{uc}^{\text{Dis}}_{s,t,n}$, and $\text{uc}^{\text{Sim}}_{s,t,n}$ denote the binary decision variables indicating charging, discharging, and simple cycle states.

$$\text{uc}^{\text{Ch}}_{s,t,n} + \text{uc}^{\text{Dis}}_{s,t,n} + \text{uc}^{\text{Sim}}_{s,t,n} \leq 1\,, \qquad \forall\, s, t, n \tag{6}$$

In terms of limiting the charging power, the charging power must not exceed a maximum charging power of $\text{PC}^{\text{C}}_{\text{max}}$ as

described in (7). Similarly, the discharging and simple cycle power have been set not to exceed a maximum capacity of PC_{max}^{EXP}, as denoted by (8) and (9).

$$0 \le PC_{s,t,n}^{Ch} \le PC_{max}^{C} \times uc_{s,t,n}^{Ch}, \quad \forall s,t,n \tag{7}$$
$$0 \le PC_{s,t,n}^{Dis} \le PC_{max}^{EXP} \times uc_{s,t,n}^{Dis}, \quad \forall s,t,n \tag{8}$$
$$0 \le PC_{s,t,n}^{Sim} \le PC_{max}^{EXP} \times uc_{s,t,n}^{Sim}, \quad \forall s,t,n \tag{9}$$

At each time segment, the energy content of CAES is calculated via (10). Here, Er denotes the energy ratio of the CAES; in addition, the energy content is limited to be within EC_{min} and EC_{max}, as stated in (11).

$$EC_{s,t,n} = EC_{s,t-1,n} + PC_{s,t,n}^{Ch} - PC_{s,t,n}^{Dis} \times Er, \quad \forall s,t,n \tag{10}$$
$$EC_{min} \le EC_{s,t,n} \le EC_{max}, \quad \forall s,t,n \tag{11}$$

During the discharging process, a considerable amount of heat is produced, which is formulated by (12), where $\gamma_{CAES}^{Dis,E2T}$ and $\gamma_{CAES}^{Sim,E2T}$ represent electrical to thermal output coefficients in discharging and simple cycle modes. If recovered efficiently [19], this heat energy could realize end-users thermal demands leading to more efficient thermal operation of the CAES plants. Nevertheless, in terms of satisfying thermal demands, the high dependency between the discharging process and the heat recovered could be challenging when relying on CAES alone. Eventually, the natural gas consumed $NG_{s,t,n}^{CAES}$ is limited to less than NG_{max}^{CAES} as expressed in (13).

$$H_{s,t,n}^{CAES} = PC_{s,t,n}^{Dis} \times \gamma_{CAES}^{Dis,E2T} + PC_{s,t,n}^{Sim} \times \gamma_{CAES}^{Sim,E2T}, \quad \forall s,t,n \tag{12}$$
$$0 \le NG_{s,t,n}^{CAES} \le NG_{max}^{CAES}, \quad \forall s,t,n \tag{13}$$

C. BATTERY ENERGY STORAGE SYSTEM MODEL

The BESS noticeably mitigates the operation cost and emission generated. Consequently, BESS charging and discharging model is established in this section. The SOC at each time segment t is denoted in (14). Additionally, γ_{BESS}^{Ch} and γ_{BESS}^{Dis} denote the charging and discharging efficiency, respectively.

$$SOC_{s,t,n}^{BESS} = SOC_{s,t-1,n}^{BESS} + PB_{s,t,n}^{Ch,BESS} \times \gamma_{BESS}^{Ch} - \frac{PB_{s,t,n}^{Dis,BESS}}{\gamma_{BESS}^{Dis}}, \quad \forall s,t,n \tag{14}$$

The operation constraints of the BESS are fully considered in (15)-(18). To limit the charging and discharging power, (15) and (16) are set which CR represents the power rate limit of the BESS in kW. Moreover, $b_{s,t,n}^{Ch}$ and $b_{s,t,n}^{Dis}$ are binary variables, respectively, indicating the charging and discharging states at time t.

$$0 \le PB_{s,t,n}^{Ch} \le b_{s,t,n}^{Ch} \times CR, \quad \forall s,t,n \tag{15}$$
$$0 \le PB_{s,t,n}^{Dis} \le b_{s,t,n}^{Dis} \times CR, \quad \forall s,t,n \tag{16}$$

The SOC is not allowed to exceed the maximum and minimum values of SOC_{max}^{BESS} and SOC_{min}^{BESS}, respectively which is illustrated by (17). Eventually, to ensure that the simultaneous charge and discharge are forbidden, (18) is established.

$$SOC_{min}^{BESS} \le SOC_{s,t,n} \le SOC_{max}^{BESS}, \quad \forall s,t,n \tag{17}$$
$$b_{s,t,n}^{Ch} + b_{s,t,n}^{Dis} \le 1, \quad \forall s,t,n \tag{18}$$

D. PLUG-IN ELECTRIC VEHICLE MODEL

PEV parking lots could be highly beneficial in promoting system stability and profit. However, the stochastic nature of the PEVs represented in the distance traveled, arrival and departure times, initial SOC, and driving habits during the different seasons could pose severe issues regarding the planning of the charge and discharge of PEVs. Accordingly, this section is broken into three subsections explaining the stochastic nature of PEV, the modeling of PEVs' batteries, and finally, the constraints restricting PEVs' scheduling scheme.

1) STOCHASTIC NATURE OF PEV

Initially, a logarithmic distribution function is represented to depict the daily driving distance as follows [34]:

$$f_{Dis,j}(x) = \frac{1}{\sqrt{2\pi}\sigma_{Dis,t}x} exp\left(-\frac{\left(lnx - \mu_{Dis,t}\right)^2}{2{\sigma_{Dis,t}}^2}\right), \tag{19}$$

where $\sigma_{Dis,t}$ and $\mu_{Dis,t}$ denote the mean, and standard deviation of the distance traveled at time t, respectively. Afterward, the arrival time of each PEV is formulated using the normal distribution function as follows [35]:

$$f_{Ar,t,j}(t_{Ar}) = \frac{1}{\sqrt{2\pi}\sigma_{Ar,t}} exp\left(-\frac{\left(t_{Ar} - \mu_{Ar,t}\right)^2}{2{\sigma_{Ar,t}}^2}\right) \tag{20}$$

Here, $\sigma_{Ar,t}$ and $\mu_{Ar,t}$ represent the mean and standard deviation of the arrival time at t. It is worth mentioning that each PEV is allowed to be plugged into the system for 12 hours and then leave the parking lot with a minimum SOC of 75%, consequently ensuring the owner's satisfaction with participating in the vehicle-to-grid scheme (V2G). Eventually, the initial SOC of each PEV entering the parking lot is considered. The initial SOC depends on the distance traveled and the all-electric range. The initial SOC can be computed as follows:

$$SOC_{initial,j} = \begin{cases} \dfrac{AMR_j - Distance_j}{AMR_j}, & 0 < Distance_j < AMR_j \\ 20\%, & Distance_j > 0.8 \times AMR_j \end{cases} \tag{21}$$

where $Distance_j$ and AMR_j denote the traveling distance and all-electric range for the *jth* PEV. As a safety precaution against battery degradation, the depth of charge is set not to exceed 80%. The AMR is calculated by (22) where $C_{batt,j}$ denotes the battery capacity of the *jth* PEV and $E_{con/mile,j}$

represents the energy consumption per mileage.

$$\mathrm{AMR}_j = \frac{C_{\mathrm{batt},j}}{E_{\mathrm{con/mile},j}} \tag{22}$$

2) MODELING OF PEV BATTERY

After a charging/discharging cycle, the updated SOC of the PEV battery denoted as $\mathrm{SOC}^{\mathrm{PEV}}_{s,t,j}$, could be calculated from the following:

$$\mathrm{SOC}^{\mathrm{PEV}}_{s,t,j} = \mathrm{SOC}^{\mathrm{PEV}}_{s,t-1,j} + \mathrm{PB}^{\mathrm{Ch,PEV}}_{s,t,j} \times \gamma^{\mathrm{Ch}}_{\mathrm{PEV}} - \frac{\mathrm{PB}^{\mathrm{Dis,PEV}}_{s,t,j}}{\gamma^{\mathrm{Dis}}_{\mathrm{PEV}}}, \ \forall s,t,j \tag{23}$$

Here, $\mathrm{PB}^{\mathrm{Ch,PEV}}_{s,t,j}$ and $\mathrm{PB}^{\mathrm{Dis,PEV}}_{s,t,j}$ represent the charging and discharging power for the *jth* PEV at time t for scenario s, respectively. In addition, the charging and discharging efficiencies of the *jth* PEV are represented as $\gamma^{\mathrm{Ch}}_{\mathrm{PEV}}$ and $\gamma^{\mathrm{Dis}}_{\mathrm{PEV}}$, respectively.

Generally, the parking lot charging and discharging capacity will be partitioned among PEVs at each time segment. As a result, several aspects, such as arrival time, departure time, current SOC, and battery capacity, should be considered while prioritizing the distribution process. Thereby, the charging and discharging power of the *jth* PEV at each time segment t and scenario s could be modeled as [36].

$$\mathrm{PB}^{\mathrm{Ch,PEV}}_{s,t,j} = \frac{(C_{\mathrm{batt},j} - \mathrm{SOC}^{\mathrm{PEV}}_{s,t,j} \times C_{\mathrm{batt},j}) \times P_{\mathrm{LOT},t,s}}{t_{\mathrm{rem},j} \times \sum_{k=1}^{\mathrm{J}} \frac{1}{t_{\mathrm{rem},k}} (C_{\mathrm{batt},k} - \mathrm{SOC}^{\mathrm{PEV}}_{t,k,s} \times C_{\mathrm{batt},k})} \tag{24}$$

$$\mathrm{PB}^{\mathrm{Dis,PEV}}_{s,t,j} = \frac{t_{\mathrm{rem},n}(C_{\mathrm{batt},j} \times \mathrm{SOC}^{\mathrm{PEV}}_{s,t,j}) \times P_{\mathrm{LOT},t,s}}{\sum_{k=1}^{K} \frac{1}{t_{\mathrm{rem},k}} (\mathrm{SOC}^{\mathrm{PEV}}_{t,k,s} \times C_{\mathrm{batt},k})} \tag{25}$$

where $t_{\mathrm{rem},j}$ represents the remaining time in the parking lot, which could be calculated knowing the entrance ($t_{\mathrm{arr},j}$) and exit times ($t_{\mathrm{exit},j}$) as follows:

$$t_{\mathrm{rem},j} = t_{\mathrm{exit},j} - t_{\mathrm{arr},j} \tag{26}$$

3) PEV CONSTRAINTS

The PEV scheduling scheme should undergo some technical constraints. The energy balance of the batteries is realized by (27), where $E^{\mathrm{PEV}}_{s,t,j}$ denotes the electric energy stored in *jth* PEV at t. Moreover, the energy stored should be restricted to an assured range, as reflected in (28).

$$E^{\mathrm{PEV}}_{s,t,j} = E^{\mathrm{PEV}}_{s,t-1,j} + \mathrm{PB}^{\mathrm{Ch,PEV}}_{s,t,j} \times \gamma^{\mathrm{Ch}}_{\mathrm{PEV}} \times \Delta T - \frac{\mathrm{PB}^{\mathrm{Dis,PEV}}_{s,t,j} \times \Delta T}{\gamma^{\mathrm{Dis}}_{\mathrm{PEV}}}, \ \forall s,t,j \tag{27}$$

$$\mathrm{E}^{\mathrm{PEV}}_{\mathrm{min}} \le \mathrm{E}^{\mathrm{PEV}}_{s,t,j} \le \mathrm{E}^{\mathrm{PEV}}_{\mathrm{max}}, \quad \forall s,t,j \tag{28}$$

The charging power is restricted to be within a maximum of $\mathrm{PB}^{\mathrm{Ch,PEV}}_{\mathrm{max}}$ with a binary indicator $\mathrm{I}^{\mathrm{Ch,PEV}}_{\mathrm{s,t,j}}$ indicating that the *jth* PEV is charging at a specific time segment *t,* as shown by (29). Similarly, the discharging power is maintained within a maximum discharging power of $\mathrm{PB}^{\mathrm{Dis,PEV}}_{\mathrm{max}}$ with a binary indicator $\mathrm{I}^{\mathrm{Dis,PEV}}_{s,t,j}$ indicating that the *jth* PEV is discharging at a specific time segment t as demonstrated by (30). The SOC of the PEV is then limited to falling within $\mathrm{SOC}^{\mathrm{PEV}}_{\mathrm{max}}$ and $\mathrm{SOC}^{\mathrm{PEV}}_{\mathrm{min}}$ limits as shown in (31). Nevertheless, simultaneous charging/discharging is strictly prohibited by (32).

$$0 \le \mathrm{PB}^{\mathrm{Ch,PEV}}_{t,j,s} \le \mathrm{PB}^{\mathrm{Ch,PEV}}_{\mathrm{max}} \times I^{\mathrm{Ch,PEV}}_{s,t,j}, \ \forall s,t,j \tag{29}$$

$$0 \le \mathrm{PB}^{\mathrm{Dis,PEV}}_{t,j,s} \le \mathrm{PB}^{\mathrm{Dis,PEV}}_{\mathrm{max}} \times I^{\mathrm{Dis,PEV}}_{s,t,j}, \ \forall s,t,j \tag{30}$$

$$\mathrm{SOC}^{\mathrm{PEV}}_{\mathrm{min}} \le \mathrm{SOC}^{\mathrm{PEV}}_{s,t,j} \le \mathrm{SOC}^{\mathrm{PEV}}_{\mathrm{max}}, \quad \forall s,t,j \tag{31}$$

$$0 \le I^{\mathrm{Ch,PEV}}_{s,t,j} + I^{\mathrm{Dis,PEV}}_{s,t,j} \le 1, \quad \forall s,t,j \tag{32}$$

E. DEMAND RESPONSE PROGRAM MODEL

DRP is considered one effective DSMP program strategy that allows end-users to participate actively in the electricity market. Generally, the participants would modify their consumption patterns mitigating peak load and filling the valleys in response to a price signal. However, this would impose discomfort affecting participants' tendency to be engaged in the DRP. The discomfort cost resulting from load pattern change is formulated as follows [40]:

$$C_{\mathrm{eleDR}} = \sum_{t=1}^{T} \begin{pmatrix} \pi^{\mathrm{ele,Down}}_{\mathrm{DRP}} \times P^{\mathrm{ele,Down}}_{t,s} \\ +\pi^{\mathrm{ele,Up}}_{\mathrm{DRP}} \times \mathrm{P}^{\mathrm{ele,Up}}_{t,s} \end{pmatrix} \times \Delta \mathrm{T} \tag{33}$$

where $\pi^{\mathrm{ele,Down}}_{\mathrm{DRP}}$ and $\pi^{\mathrm{ele,Up}}_{\mathrm{DRP}}$ denote the ascending and descending costs of electric DRP and the variables $P^{\mathrm{ele,Down}}_{\mathrm{t,s}}$ and $\mathrm{P}^{\mathrm{ele,Up}}_{\mathrm{t,s}}$ define the electric power descended and ascended by DRP, respectively. Typically, the electric DRP constraints are established as follows:

$$\sum_{t}^{T} P^{\mathrm{ele,Up}}_{t,s} = \sum_{t}^{T} P^{\mathrm{ele,Down}}_{t,s} \tag{34}$$

$$0 \le P^{\mathrm{ele,Up}}_{t,s} \le \mathrm{Mr}^{\mathrm{ele,Up}} \times P^{\mathrm{ele}}_{t,s} \times I^{\mathrm{ele,Up}}_{t,s} \tag{35}$$

$$0 \le P^{\mathrm{ele,Down}}_{t,s} \le \mathrm{Mr}^{\mathrm{ele,Down}} \times P^{\mathrm{ele}}_{t,s} \times I^{\mathrm{ele,Down}}_{t,s} \tag{36}$$

The sum of electric power transferred up and down is restricted as in (34). The upper limits of up-down electric power charge are represented in (35) and (36) where $\mathrm{Mr}^{\mathrm{ele,Up}}$ and $\mathrm{Mr}^{\mathrm{ele,Down}}$ denote the maximum up-down electric power ratios transferred. According to DRP contract constraints, the controllable demands could be increased up to 50% of the base consumers' demand $P^{\mathrm{ele}}_{t,s}$ during low electricity prices. Furthermore, for a high electricity price period, the controllable demands could be decreased up to 50%, as tabulated in Table 2.

Eventually, the inapplicability of simultaneous up-down electric charge transfer is addressed in (37). $I^{\mathrm{ele,Up}}_{t,s}$ represents a binary variable that indicates the increment in the electricity demand; when equal to 1, it denotes an increase in electricity demand in period t; otherwise, it is equal to 0. Similarly, $I^{\mathrm{ele,Down}}_{t,s}$ denotes a decreased status in electricity demand in

period t; otherwise, it equals 0.

$$0 \leq I_{t,s}^{\text{ele,Up}} + I_{t,s}^{\text{ele,Down}} \leq 1 \tag{37}$$

F. AIR AND HOT WATER DEMAND MODEL

In this work, air temperature regulation and hot water are the main thermal demands that must be satisfied. To calculate the households' temperature, a straightforward equation was proven in [37]. The indoor and outdoor temperature differential is addressed, which leads to a heat energy transfer from the hotter to colder matter taking place as follows:

$$T_{s,t,n}^{\text{indoor}} = T_{s,t-1,n}^{\text{indoor}} \times e^{\frac{-1}{R \times C_{AIR}}} + \left(R \times H_{s,t,n}^{\text{AIR}} + T_{s,t,n}^{\text{outdoor}}\right) \times \left(1 - e^{\frac{-1}{R \times C_{AIR}}}\right) \tag{38}$$

As it is clearly indicated from the previous equation, the indoor households' temperature $T_{t,s}^{\text{indoor}}$ mainly depends on outdoor households' temperature $T_{t,s}^{\text{outdoor}}$, thermal energy transferred into household $H_{t,s}^{\text{AIR}}$, heat resistance of the walls R, and specific heat of the air C_{AIR}.

For hot water demand satisfaction, cold water is blended with hot water in the storage tank leading to a state of temperature equilibrium. In this study, it is assumed that hot water consumed is constantly being substituted with cold water having the same volume. The dynamic of the water flow is beyond the scope of this paper. The water temperature at each time step $T_{s,t,n}^{\text{WS}}$ is obtained as follows [38]:

$$T_{s,t,n}^{\text{WS}} = \frac{\left[V_{s,t-1,n}^{\text{COLD}} \times \left(T^{\text{CW}} - T_{t-1,s}^{\text{WS}}\right) + V^{\text{WS}} \times T_{s,t-1,n}^{\text{WS}}\right]}{V^{WS}} + \frac{H_{s,t,n}^{\text{WS}}}{V^{\text{WS}} \times C_W} \tag{39}$$

The first term of this equation elaborates on the temperature balance in the tank, which depends on the volume of the cold water entering the tank at time t and scenario s which is denoted as $V_{s,t,n}^{\text{COLD}}$; the temperature of cold water is defined as T^{CW}; the volume of hot water storage is denoted by V^{WS}. The second term relates to stored water temperature calculated knowing the thermal energy transferred to the hot water storage at time t depicted as $H_{s,t,n}^{\text{WS}}$; the volume of hot water storage; the specific heat of water is defined by C_{W}.

It is primarily apparent that customer satisfaction must be considered; that is, the satisfaction strategy should be enforced to a reasonable limit as established in (40) and (41).

$$T_{\min}^{\text{WS}} \leq T_{s,t,n}^{\text{WS}} \leq T_{\max}^{\text{WS}}, \quad \forall s, t, n \tag{40}$$

$$T_{\min}^{\text{indoor}} \leq T_{s,t,n}^{\text{indoor}} \leq T_{\max}^{\text{indoor}}, \quad \forall s, t, n \tag{41}$$

G. THERMAL ENERGY STORAGE MODEL

As a result of humanity's massive thermal energy consumption, technological advancement regarding thermal energy storage and planning needs to be addressed. Accordingly, TES has emerged globally as a critical thermal energy management function [39]. Thereby, the applicability of this technology has been analyzed in an EH-based microgrid to achieve the thermal equilibrium whenever the unbalance between generation and consumption is triggered; this is illustrated as follows:

$$E_{s,t,n}^{\text{TES}} = E_{s,t-1,n}^{\text{TES}} + \left(P_{s,t,n}^{\text{TES,in}} \times \sigma_{in} - \frac{P_{s,t,n}^{\text{TES,DR}}}{\sigma_{\text{DR}}}\right), \quad \forall s, t, n \tag{42}$$

Here, and for the *nth* EH, $E_{s,t,n}^{\text{TES}}$ denotes the thermal energy content of the TES in kWh. Additionally, $H_{s,t,n}^{\text{in}}$ and $H_{s,t,n}^{\text{DR}}$ represent the injected and drawn thermal energy to/from the TES. The efficiency of the injection and drawing processes has been denoted by σ_{in} and σ_{DR}, respectively.

To assure a stable and reliable operation, the operation of the TES is restricted within a defined limit illustrated by (43) and (44). That is to say, the injected and drawn heat energy is not allowed to exceed a maximum value of $P_{\max}^{\text{TES,in}}$ and $P_{\max}^{\text{TES,DR}}$, respectively. The binary variables $u_{s,t,n}^{\text{in}}$ and $u_{s,t,n}^{\text{DR}}$ denote the heat energy injection and drawing states of the TES.

$$0 \leq P_{s,t,n}^{\text{TES,in}} \leq P_{max}^{\text{TES,in}} \times u_{s,t,n}^{\text{in}}, \quad \forall s, t, n \tag{43}$$

$$0 \leq P_{s,t,n}^{\text{TES,DR}} \leq P_{max}^{\text{TES,DR}} \times u_{s,t,n}^{\text{DR}}, \quad \forall s, t, n \tag{44}$$

To prevent the simultaneous injection and draw of heat energy, (45) has been established. Moreover, the stored energy should not exceed a maximum and minimum threshold of $E_{\min}^{\text{TES}}$ and $E_{\max}^{\text{TES}}$, respectively as is evident by (46).

$$u_{s,t,n}^{\text{DR}} + u_{s,t,n}^{\text{in}} \leq 1, \quad \forall s, t, n \tag{45}$$

$$E_{\min}^{\text{TES}} \leq E_{s,t,n}^{\text{TES}} \leq E_{\max}^{\text{TES}}, \quad \forall s, t, n \tag{46}$$

IV. UNCERTAINTY MODELING

This study comprehensively analyzes the impact of uncertainties associated with photovoltaic systems, wind turbines, electrical and thermal demands, and electricity market prices. To provide a more in-depth analysis; this section is divided into subsections as follows:

A. PHOTOVOLTAIC SYSTEM

PV module output power is determined mainly by solar irradiance, which comes with a significant degree of unpredictability. Accordingly, to model this uncertainty, the beta probability distribution function (PDF), which depicts a bimodal distribution, is regularly employed and formulated as follows [18]:

$$f_{\text{beta}}(\emptyset) = \begin{cases} \dfrac{\Gamma(\alpha^{\text{sr}} + \beta^{\text{sr}})}{\Gamma(\alpha^{\text{sr}})\Gamma(\beta^{\text{sr}})} \times \emptyset^{(\alpha^{\text{sr}}-1)} \times (1-\emptyset)^{(\beta^{\text{sr}}-1)}, \\ \qquad 0 \leq \emptyset \leq 1, \quad \alpha^{\text{sr}} \geq 0, \ \beta^{\text{sr}} \geq 0 \\ 0, \qquad \text{otherwise} \end{cases} \tag{47}$$

Here, $\emptyset$ represents the solar irradiance in kW/m2. In addition, α^{sr} and β^{sr} denote the shape factor parameters of beta

distribution which are dependent on the mean (μ^{sr}) and standard deviation (σ^{sr}) as follows:

$$\beta^{\mathrm{sr}} = (1-\mu^{\mathrm{sr}}) \times \left(\frac{\mu^{\mathrm{sr}} \times (1+\mu^{\mathrm{sr}})}{\sigma^{sr\,2}} - 1 \right) \tag{48}$$

$$\alpha^{\mathrm{sr}} = \frac{\mu^{\mathrm{sr}} \times \beta^{\mathrm{sr}}}{1-\mu^{\mathrm{sr}}} \tag{49}$$

Afterward, the power output for the lth PV module for scenario s is calculated as follows [33]:

$$P^{\mathrm{PV}}_{s,t,l} = \sigma^{\mathrm{PV}} \times S^{\mathrm{PV}} \times \emptyset_{s,t,l} \times \left(1 - 0.005\left(T^{\mathrm{Am}} - 25\right)\right), \quad \forall\, s, t, l \tag{50}$$

Here, σ^{PV}, S^{PV}, and T^{Am} denote the efficiency, surface area, and ambient temperature of PV modules, respectively.

B. WIND TURBINE

To simulate the behavior of wind speed under uncertainty utilizing a statistical approach, Rayleigh PDF, which is a particular derivative of Weibull PDF in which the shape factor K is equal to 2 [6], is employed and expressed as follows:

$$f_W\left(V^{\mathrm{WT}}\right) = \frac{K}{C} \times \left(\frac{V^{\mathrm{WT}}}{C}\right)^{(K-1)} \times exp\left(-\left(\frac{V^{\mathrm{WT}}}{C}\right)^{K}\right) \tag{51}$$

In this equation, the scale factor C is equal to $\mathrm{v}_{avg}/0.9$, in which v_{avg} denotes the incident average wind speed at a particular site. V^{WT} represents wind speed in (m/s). Afterward, a piecewise cubic power curve can be exploited to compute the output power of the mth wind turbine as a function of ambient wind speed formulated as:

$$P^{\mathrm{WT}}_{s,t,m} = \begin{cases} 0 & V^{\mathrm{WT}}_{s,t,m} \le V_{\mathrm{CI}} \\ P^{\mathrm{WT}}_{\mathrm{RATED}} \times \left(\dfrac{V^{\mathrm{WT}}_{s,t,m} - V_{\mathrm{CI}}}{V_{\mathrm{RATED}} - V_{\mathrm{CI}}}\right)^3 & V_{\mathrm{CI}} \le V^{\mathrm{WT}}_{s,t,m} \le V_{\mathrm{CR}} \\ P^{\mathrm{WT}}_{\mathrm{RATED}} V_{\mathrm{CR}} \le V^{\mathrm{WT}}_{s,t,m} \le V_{\mathrm{CO}} & \\ 0 & V^{\mathrm{WT}}_{s,t,m} \ge V_{\mathrm{CO}} \end{cases} \tag{52}$$

Here, V_{CI}, V_{CR}, and V_{CO} are cut-in, rated, and cut-out wind speeds, respectively. $P^{\mathrm{WT}}_{\mathrm{RATED}}$ is the rated power output in kW.

C. ELECTRICAL AND THERMAL DEMANDS

Generally, the uncertainty associated with the electrical and thermal demand is established by the normal PDF [40] as follows:

$$f_{\mathrm{dem}}\left(L_{\mathrm{dem}}\right) = \frac{1}{\sqrt{2\pi}\,\sigma_{\mathrm{dem}}} exp\left(-\frac{\left(L_{\mathrm{dem}} - \mu_{\mathrm{dem}}\right)^2}{2\sigma^2_{\mathrm{dem}}}\right) \tag{53}$$

Here, $f_{\mathrm{dem}}\left(L_{\mathrm{dem}}\right)$ denotes PDF of the demand uncertainty. μ_{dem} and σ_{dem} represent the mean and standard deviation of the historical demand data, respectively.

D. ELECTRICAL PRICE

The electricity price tariff has been upgraded to the time of use tariff (TOT) [23]. Consequently, significant reductions in capital investments and transmission costs have been obtained. In fact, TOT constantly encourages end-users to shave and reduce peak power. To simulate the uncertainty of the electric tariff; a normal PDF is employed as follows:

$$P\left(X = x_{\mathrm{Pr}} | \mu_{\mathrm{Pr}}, \sigma^2_{\mathrm{Pr}}\right) = f_{\mathrm{Price}}\left(x_{\mathrm{Pr}}\right) = \frac{1}{\sqrt{2\pi}\,\sigma_{\mathrm{Pr}}} exp\left(-\frac{\left(x_{\mathrm{Price}} - \pi\right)^2}{2\sigma^2_{\mathrm{Pr}}}\right) \tag{54}$$

For electricity price variable x_{Pr}, the parameters σ_{Pr} and μ_{Pr} denote the standard deviation and average value, respectively.

V. ELECTRIC, GAS AND HEAT FLOW CONDITIONS AND EQUILIBRIUM

The electrical power flow $P^{\mathrm{elec}}_{i,j,t,s}$ from the *ith* to the *jth* bus is represented as follows [32]:

$$P^{\mathrm{elec}}_{i,j,t,s} = V_{i,t,s}V_{j,t,s} \times \left(G_{i,j}cos\theta_{i,j,s} + B_{i,j}sin\theta_{i,j,s}\right) - G_{i,j}V^2_{i,t,s} \tag{55}$$

Here, $V_{i,t,s}$ and $V_{j,t,s}$ are the voltages of the buses i and j, respectively. Additionally, $G_{i,j}$ and $B_{i,j}$ denote the conductance and the substance of the branch ij, respectively. The angle difference between bus voltages i and j is indicated as $\theta_{i,j,s}$. For the electric power balance achieved for each bus in the IEEE-33 system, the following equation is established:

$$P^{\mathrm{elec}}_{G,i,t,s} - P^{\mathrm{elec}}_{D,i,t,s} \pm P_{\mathrm{LOT},t,s} \pm P^{\mathrm{elec}}_{\mathrm{EH},n,t,s} - \sum_{j\in i} P^{\mathrm{elec}}_{i,j,t,s} = 0, \tag{56}$$

where, $P^{\mathrm{elec}}_{G,i,t,s}$ and $P^{\mathrm{elec}}_{D,i,t,s}$ indicate the generated and demanded power for bus i. Moreover, $P^{\mathrm{elec}}_{\mathrm{EH},n,t,s}$ denotes the aggregate power of the electric equipment of the *nth* EH. Generally, natural gas flowing through the natural gas network with i and j branches are illustrated as follows [32]:

$$N^{\mathrm{gas}}_{i,j,t,s} = k_{i,j,t,s}s_{i,j,t,s} \times \sqrt{\left|\rho^2_{i,t,s} - \rho^2_{j,t,s}\right|}$$
$$\text{where} \quad s_{i,j,t,s} = \begin{cases} 1 & \rho_{i,t,s} \ge \rho_{j,t,s} \\ -1 & \text{otherwise} \end{cases} \tag{57}$$

Here, ρ_i and ρ_j correspondingly indicate the pressure of the down and up streams. Moreover, the transmission coefficient between nodes i and j is denoted as $k_{i,j}$. Finally, the gas flow balance at node x, which mainly depends on gas generation $N^{\mathrm{gas}}_{G,i,t,s}$ and consumption $N^{\mathrm{gas}}_{D,j,t,s}$, is established as follows:

$$N^{\mathrm{gas}}_{G,i,t,s} - N^{\mathrm{gas}}_{D,i,t,s} - \sum_{j\in i} N^{\mathrm{gas}}_{i,j,t,s} = 0 \tag{58}$$

To promote the reliability of the optimization model, it is crucial to consider the power and heat flow conditions. The power flow between the EHs and the distribution network is

bidirectional. Moreover, the PEVs are employed with V2G capability. If the power is consumed, it would be assigned to a positive value, whereas it would be negative if it is injected into the grid. The power balance condition within each EH is guaranteed by applying (59), where $\text{PGrid}_{s,t,n}$ and $\text{Demand}_{s,t,n}$ represent the grid power and electrical demand for t under scenarios s for the *nth* EH.

$$P^{\text{DiCs}}_{s,t,n} + PC^{\text{Sim}}_{s,t,n} + PB^{\text{Dis,BESS}}_{s,t,n} + P^{\text{PV}}_{s,t,l} + P^{\text{WT}}_{s,t,m} + \text{PGrid}_{s,t,n} + P^{\text{ele,Down}}_{s,t} \geq \text{Demand}_{s,t,n} + \text{PC}^{\text{Ch}}_{s,t,n} + PB^{\text{Ch,BESS}}_{s,t,n} + P^{\text{ele,Up}}_{s,t}, \ \forall s, t, n, l, m \tag{59}$$

To meet the heat flow equilibrium for each time segment and under each scenario, (60) is set as follows:

$$H^{\text{CAES}}_{s,t,n} + H^{\text{DR}}_{s,t,n} \geq H^{\text{AIR}}_{s,t,n} + H^{\text{WS}}_{s,t,n} + H^{\text{in}}_{s,t,n} \forall s, t, n \tag{60}$$

VI. SOLUTION ALGORITHM

In this study, it is desired to minimize the operation cost and the emissions by optimizing the decision variables to effectively schedule the proposed multi-carrier EH-based microgrid framework. For this purpose, the multi-objective grey wolf optimizer (MOGWO) is employed. Like other metaheuristic algorithms, a population or search agents are generated randomly, mainly depicting the social leadership of grey wolves chasing and hunting their prey. Accordingly, the critical parameters that need to be set are alpha, beta, and delta (α, β, and δ) leadership wolves. Thus, search agents tend to converge from/towards the prey according to well-established position equations until optimality is fulfilled.

Concerning having a rapid convergence to solutions and obtaining highly competitive results, MOGWO can be advantageous since it has superiority in the exploration phase compared to other well-known algorithms. For instance, the multi-objective particle swarm optimization algorithm (MOPSO) was proven to have fast convergence characteristics that make it more likely to terminate with false Pareto front solutions [41]. Meanwhile, the adaptive values of the different MOGWO provide a smooth transition between the exploration and exploitation which results in convergence toward a true Pareto optimal front [42].

Once Pareto's optimal front is stored in the archive, higher-level qualitative factors should be addressed when making the final decision. The fuzzy set theory could be established to summarize the issue and locate the most effective non-dominant solution. It is noteworthy that selecting one optimal solution among the Pareto front to satisfy both objectives simultaneously could impose such a challenge. This could be related to the fact that objectives usually possess a conflicting nature with each other.

Fuzzy set theory is applied to find a trade-off between the objectives. As it is considered the most suitable function for the power system's optimal solution space, the linear membership function has been deployed in this study as follows [40]:

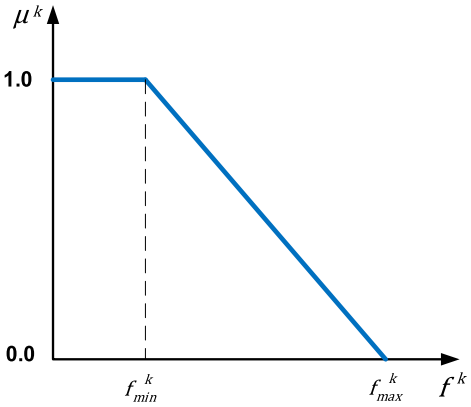

FIGURE 3. Linear membership function of the *kth* objective.

$$\mu^k_i = \begin{cases} 1 & f^k_i \leq f^k_{\min} \\ \dfrac{f^k_{\max} - f^k_i}{f^k_{\max} - f^k_{\min}} & f^k_{\min} \leq f^k_i \leq f^k_{\max} \\ 0 & f^k_i \geq f^k_{\max} \end{cases} \tag{61}$$

For the *ith* Pareto front solution and *kth* objective, μ^k_i denotes the linear membership function. Whereas the minimum and maximum values of the *kth* objective are denoted as $f^k_{\min}$ and $f^k_{\max}$, respectively. The membership function could be obtained for a set of non-dominated solutions of the multi-objective problem to have any value between 1 and zero as illustrated in Fig. 3.

Generally, as the value of the evaluated membership function increases, the degree of objective fulfillment also increases, reaching complete fulfillment at the value of 1. Otherwise, the degree of satisfaction decreases indicating a complete deficiency in meeting the objective when equal to zero. Afterward, each Pareto front is normalized using the normalized membership function as follows:

$$\mu_i = \frac{\sum_{k=1}^{N_{\text{OBJ}}} \mu^k_i}{\sum_{i=1}^{N_{PF}} \sum_{k=1}^{N_{\text{OBJ}}} \mu^k_i} \tag{62}$$

where N_{OBJ} and N_{PF} represent the total number of objectives and Pareto front solutions, respectively. After evaluating μ for each Pareto front and each objective, the values are arranged in descending order to prioritize the optimality of the solution. This would lead to assigning the solution with maximum μ to be the best compromised one.

For a more in-depth analysis of the solution process, a flowchart describing the primary steps toward the optimal schedule of the proposed scheme is illustrated in Fig. 4. The optimal scheduling of the proposed scheme is carried out considering three basic aspects, these are, (i) preparing and passing the input data, (ii) running the optimal scheduling framework, and (iii) evaluating the output data and results represented in the seasonal schedule of the CAES, BESS, TES, and PEV.

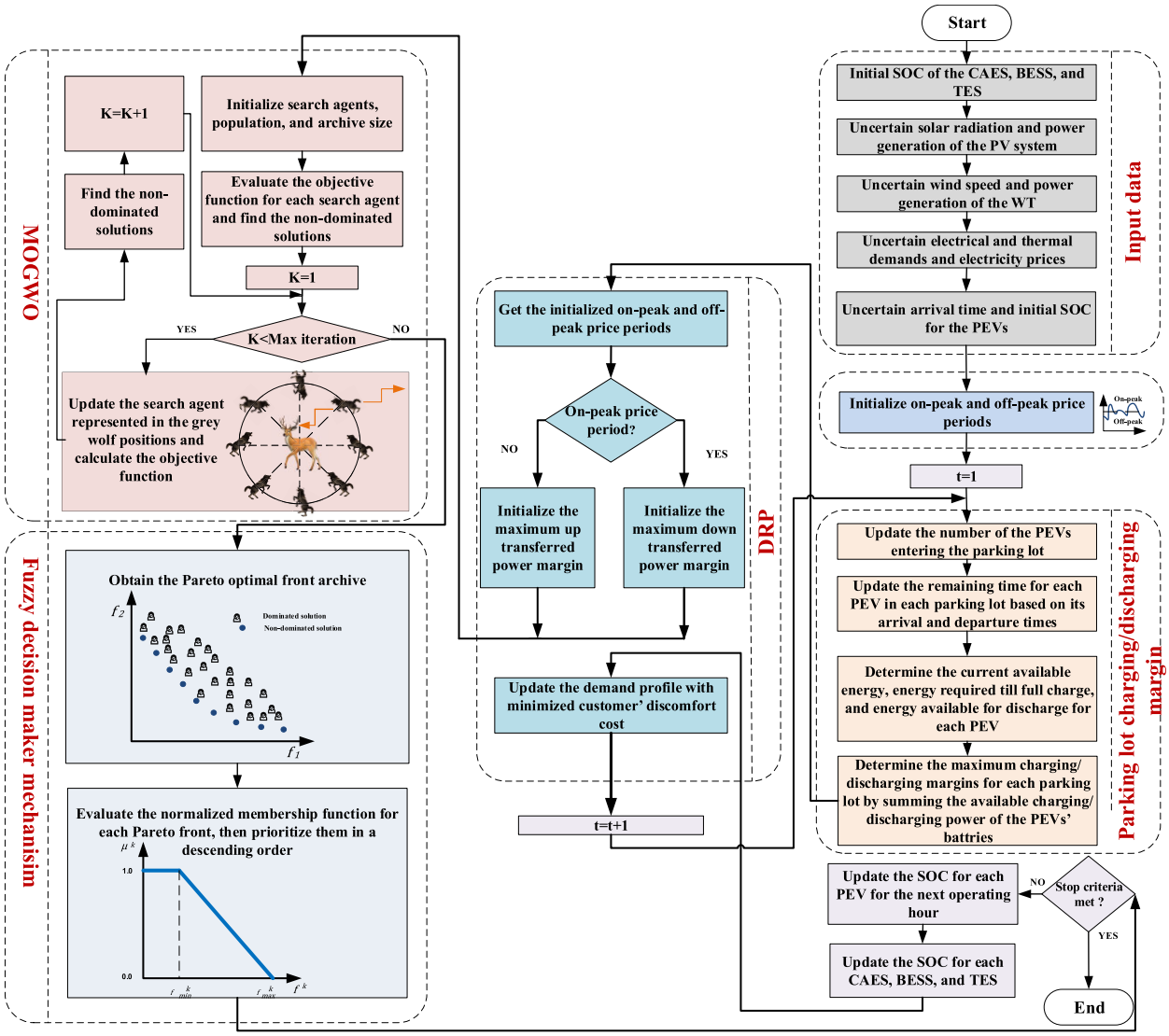

FIGURE 4. Flowchart for evaluation of the best compromised non-dominated solution for the proposed scheduling scheme of the multiple EHs-based microgrid.

For the uncertain input data collections, and after analyzing the historical data, PDFs are constructed and segmented into several scenarios assigned to their probabilities, which are then passed and sent to the optimal scheduling framework. For each hour, the number of PEVs entering the parking lots and their initial SOC is determined to establish the charging/discharging margin for these parking lots. Based on the available energy stored in the currently existing PEVs' batteries, the allowable charging/discharging power margin to be shared with the utility grid from the differed parking lots is determined as illustrated in Fig. 4. Particularly, the optimal scheduling framework implements the MOGWO to initiate the optimal scheduling process, taking the operational margins and constraints of the CAES, BESS, and TES installed at the different EH; besides, the parking lots margin placed at the different bus locations.

The MOGWO then goes through many iterations until the convergence to a set of non-dominated solutions is reached. The total number of iterations has been considered as the stop criteria of the program. It is noteworthy to mention that the Pareto optimal front is generated, and the set of non-dominated solutions is persistently obtained for every single operating hour; afterward, the best-compromised solution is selected by applying the fuzzy set theory at that specific hour. The membership function is obtained for cost and emission objectives with their non-dominated solutions μ_i^k where $k = 1, 2$; $i = 1, 2, 3, ..,$ population size, then the normalized membership function is evaluated and assigned for each one of the non-dominated solutionsμ_i where i $= 1, 2, 3, ..,$ population size. Eventually, the non-dominated solution with the highest normalized membership is selected and the corresponding results are obtained, which consist of the seasonal scheduling

TABLE 2. Technical data sets of the proposed model [32], [33], [42], [47].

CAES		Emission parameters	
EC_{max}	800 (kWh)	$\gamma_c^{CO_2}$	11.57 (g/Gj)
EC_{min}	300 (kWh)	$\gamma_c^{NO_x}$	$5e$- 3 (g/Gj)
Er	0.75	$\gamma_c^{SO_x}$	$7e$- 6 (g/Gj)
HR^{Dis}	0.004 (Gj/kWh)	$\gamma_{Net}^{CO_2}$	220 (g/kW)
HR^{Sim}	0.0105(Gj/kWh)	$\gamma_{Net}^{NO_x}$	0.019 (g/kW)
PC_{max}^{C}	100 (kW)	$\gamma_{Net}^{SO_x}$	$2.62e$- 4 (g/kW)
PC_{max}^{EXP}	150 (kW)	**TES**	
OM^{exp}	0.002 ($/kWh)	$P_{max}^{TES,in}$	200 (kW)
OM^{c}	0.002 ($/kWh)	$P_{max}^{TES,DR}$	200 (kW)
$\gamma_{CAES}^{Dis,E2T}$	0.555	E_{max}^{TES}	800 (kWh)
$\gamma_{CAES}^{Sim,E2T}$	1.458	E_{min}^{TES}	200 (kWh)
BESS		σ_{in}	0.9
CR	250 (kW)	σ_{DR}	0.9
SOC_{max}^{BESS}	1	**Hot water storage**	
SOC_{min}^{BESS}	0.2	C_W	$11.61e$- 4 (kWh/LC°)
γ_{BESS}^{Ch}	0.92	T_{max}^{WS}	80 C°
γ_{BESS}^{Dis}	0.97	T_{min}^{WS}	60 C°
PEV		T^{CW}	10 C°
SOC_{max}^{PEV}	1	V^{WS}	5000 (L)
SOC_{min}^{PEV}	0.3	**Households' parameters**	
$C_{battery}$	85 (kWh)	C_{AIR}	52.5 (kWh/C°)
γ_{PEV}^{Ch}	0.95	R	0.18 (C°/kWh)
γ_{PEV}^{Dis}	0.95	$T_{maximum}^{indoor}$	27 C°
PV / WT		$T_{minimum}^{indoor}$	22 C°
S^{PV}	15 (m^2)	μ^{NG}	0.1 (Cent/kWh)
σ^{PV}	0.13	**DRP**	
P_{RATED}^{WT}	500 (kW)	$\pi_{DRP}^{ele,Up}$	0.10 Cent/kWh)
V_{CR}	14 (m/s)	$\pi_{DRP}^{ele,Down}$	0.10(Cent/kWh)
V_{CI}	2 (m/s)	$Mr^{ele,Up}$	0.5
V_{CO}	25 (m/s)	$Mr^{ele,Down}$	0.5

of the optimized decision variables and the annual operating costs and emission amounts generated from the proposed EH-based microgrid.

VII. CASE STUDIES

Mainly, the electric distribution system used in this study consists of a typical IEEE-33 radial distribution system realizing a peak active and reactive power of 3.715 MW and 2.3 MVAR, respectively, and a substation voltage of 12.66 kV, as given in Fig. 2 [43]. In compliance with the ANSI C84.1 requirement, the buses' voltage has been restricted to have minimum and maximum voltages of 0.95 and 1.05, respectively [44].

Gas infrastructure has also been considered in the model. For the proposed multi-carrier EH-based microgrid under study, the technical parameters and constraints for the various types of integrated equipment are set as shown in Table 2.

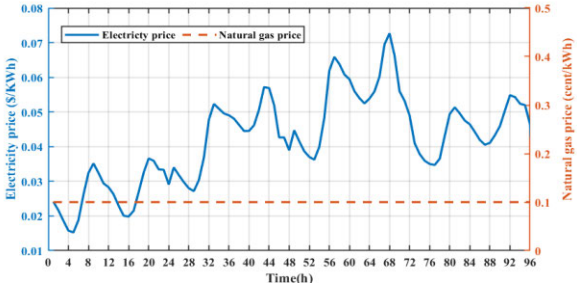

FIGURE 5. Expected market prices for electricity and natural gas.

The expected seasonal data sets of electricity price, solar irradiance, and wind speed are provided in Figs. 5 and 6 [45], [46], and [47]. Moreover, the hourly seasonal electrical generation for PV and WT systems is plotted in Fig. 7. The expected electrical and thermal demands for each EH are obtained from [31] and [45] and displayed in Fig. 9.

Tesla Model S is realized for the PEVs' battery characteristics, which have a capacity of 85 kWh [36]. The essential parameters of the PEV are tabulated in Table 2. It is assumed that 60 PEVs exist in each parking lot each season and remain there for 12 hours. Meanwhile, the PEVs can contribute to supplying the demand during the initial hours, discharging and injecting power to the parking lot, and then to the upstream grid. Nevertheless, over their final hours, PEVs regain their charging state and leave with not less than 75% SOC.

Basically, this study proposes four different case studies regarding the operation of EH-based microgrids as follows:

Case 1: The base case considers four EHs connected to the IEEE-33 bus system at four different suggested locations according to the investors' preferences, as illustrated in Fig. 2. Each EH original configuration primarily consists of CAES and TES.

Case 2: In this case, the configuration of each EH is upgraded to realize the BESS operation along with the CAES and TES.

Case 3: The DRP is employed to mitigate the operation cost.

Case 4: Parking lots are established in the predefined locations in the system, and the V2G mode is activated.

For all the mentioned cases, the objective was to mitigate the operation cost of the EHs besides the harmful emissions.

It is worth noting that CAES is the main source to satisfy electrical and thermal demands for all cases. However, the deficiency in the electrical generation is compensated by purchasing from the upstream grid, which in turn would increase the operation cost and emission amount. As progressively proceeding through the cases, the cost and emissions are expected to reduce as storage devices, that is, BESSs and PEVs besides DRP are realized. For the thermal network, TES is employed for all cases to govern the thermal generation and consumption equilibrium.

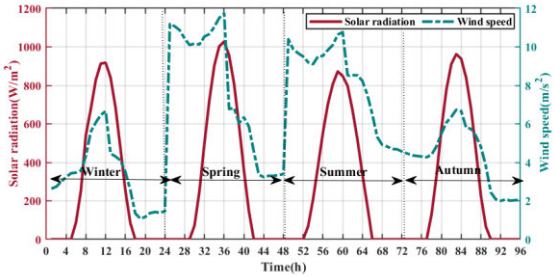

FIGURE 6. Expected hourly solar irradiance and wind speed during scheduling horizon.

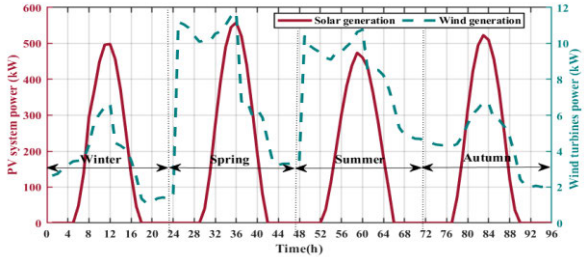

FIGURE 7. Hourly PV and wind generation during the scheduling horizon.

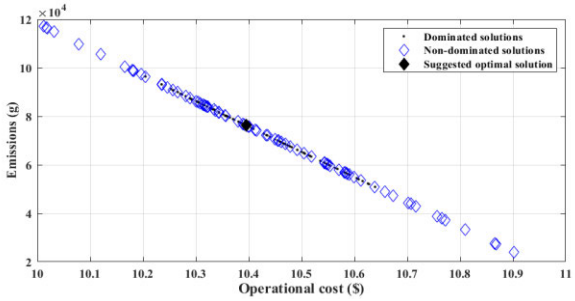

FIGURE 8. Optimal trade-off between cost and emission at one typical operation hour during the scheduling horizon.

VIII. SIMULATION RESULTS AND DISCUSSION

A. PERFORMANCE OF THE PROPOSED SCHEDULING MODEL

To analyze and evaluate the performance of the proposed scheduling model, the behavior of its various equipment is assessed based on different case studies. For the base case, the results for the Pareto optimal solution and optimal scheduling of electrical power flow for the different EHs in the microgrid are plotted in Fig. 8 and Fig. 9, respectively.

The fuzzy set theory is employed for each operating hour to select the optimal trade-off between the cost and emission objectives, as illustrated in Fig. 8. As Fig. 9 verifies, the CAESs undergo charging, discharging, and simple cycles to satisfy demand. As it is well established, CAESs start charging during low-peak price periods to store electrical energy. Once a high-peak price period is experienced, CAESs start discharging to satisfy electrical demands and reduce power purchased from the upstream grid.

Due to the fact that a simple cycle state could lead to double the fuel consumption and thus increases the operation cost, the solution algorithm avoids going through this state during the entire scheduling time horizon to satisfy the minimization of the operation cost [33].Furthermore, going through a simple cycle mode, which means operating as a conventional gas turbine, could lead to significant emissions. It is worth noting that surplus power from the CAESs is sold to the upstream grid; consequently, the power experiences a reverse flow direction, as noted during hour 12 for EH1 and 29 for EH2. This explains the bidirectional flow of the power between the grid and each EH.

For the thermal demand, the scheduling results for each EH during the study time horizon are shown in Fig. 10. Herein, the heat generated during the discharge of the CAESs and the thermal discharge of TESs are provided to satisfy the thermal demand. The discharge of the TES is plotted against the upper half of the abscissa axis; on the other hand, the charge is plotted against the lower half. Once thermal demand is low, TES starts charging mostly from discharged heat of the CAES and stores thermal energy for the next-day use. As it is evident from Fig. 10, the thermal balance is achieved between the thermal demands and generation at each operating hour.

The energy stored in the CAES for each EH is displayed in Fig. 11. As the figure reveals, CAES only provides relatively shallow cycles of discharges before reaching the minimum limit of 300 kWh; this situation is due to the fact that environmentally harmful emissions are diffused during the discharge of the CAES. The energy stored in each TES is displayed in Fig. 12. As the figure reveals, the energy stored in each TES is updated each hour according to its charging/discharging status. At the end of each day, the surplus thermal energy could be effectively stored and used the next day.

For Case 2, part of the electrical demand satisfaction is taken over by BESS alongside the CAES. As observed in Fig. 13, BESS contributes to significant discharge power compared to CAESs. This is reasonably expected as BESS charging and discharge do not contribute to pollution emissions. For instance, at 9 AM on a typical winter day for EH1, the power discharge from BESS is evaluated to be 62.1 kW compared to only 8.18 kW from CAES.

Additionally, at the same operation hour for EH2, 27.6 kW of discharge power is obtained from BESS compared to only 8.17 kW from CAES. The same principle applies to the rest EHs. The various operation cycles of CAESs and BESSs are depicted in Figs. 14 and 15, respectively. In consequence, a reduction in the operation cost and emission amount is achieved as will be comprehensively illustrated in the upcoming subsection.

To manage end-user consumption patterns, DRP is applied for Case 3, see Fig. 16. Accordingly, consumers engaged in such a program start shifting a set of residential appliances from peak to off-peak times, taking into consideration the satisfaction of the comfort preferences level of the consumer. As a result of appliance rescheduling, the aggregate peak demand would turn into a roughly flattened curve. As a consequence, the operation cost and the pollution emissions are mitigated as will be explained in the upcoming subsection.

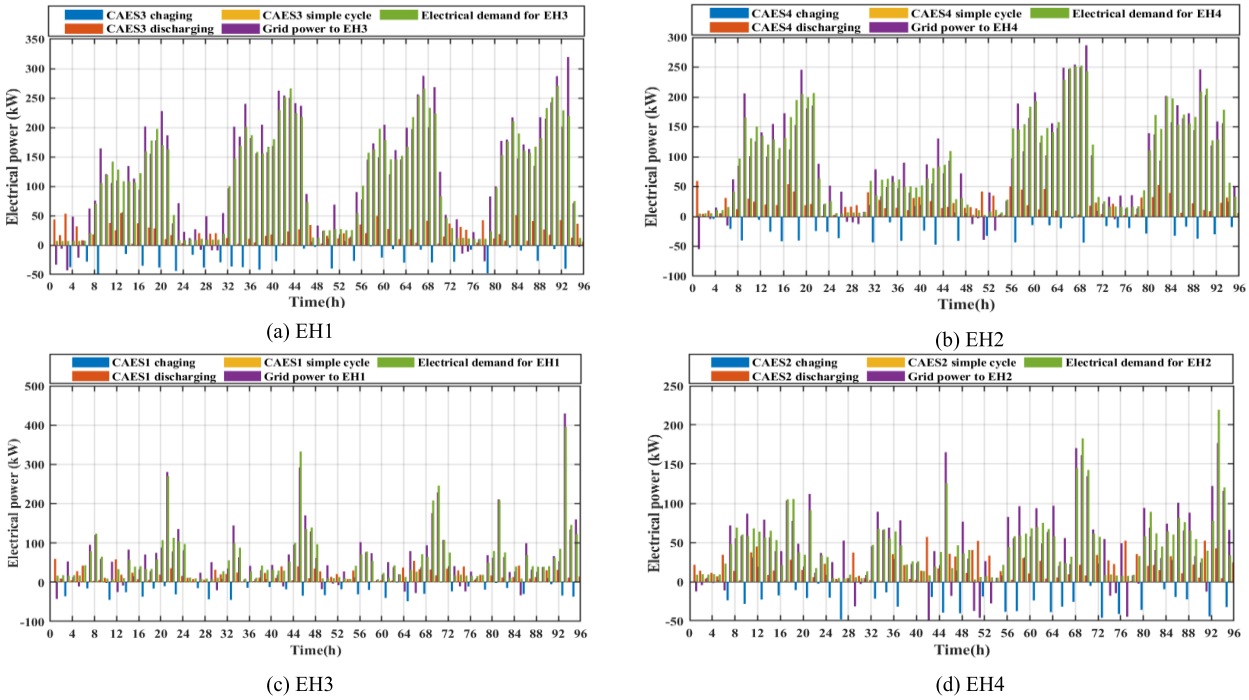

FIGURE 9. Optimal seasonal scheduling results for electrical power flow of Case 1.

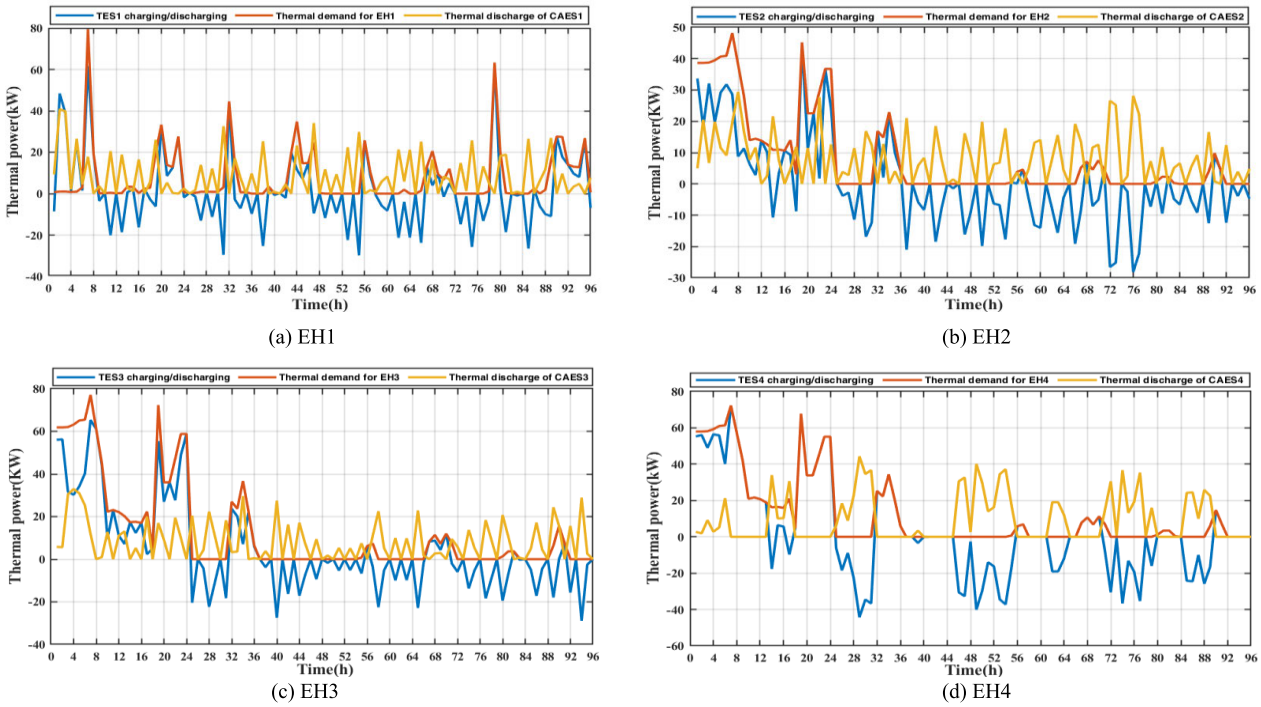

FIGURE 10. Seasonal scheduling results for thermal power flow of Case 1.

The results obtained for the optimal dispatch of electrical power under Case 4 are given in Fig. 17. For this case study, various parking lots have been incorporated into the system to optimally manage the charge and discharge of the PEVs.

For example, most PEVs arrive between 12 PM and 10 PM on a typical winter day. Once the PEV is plugged into the lots, it starts charging during its initial hours to store electrical power. Afterward, and during its middle hours, the PEV starts discharging to contribute to the satisfaction of

TABLE 3. The annual operation cost results for different case studies.

Objective	Operation cost ($)					
Season	Winter	Spring	Summer	Autumn	Total	Reduction (%)
Case 1	44278.2	26759.6	58445.0	92250.4	221553.2	-
Case 2	22896.2	1266.95	30526.3	71708.5	126397.9	42.9
Case 3	17383.1	2499.64	16388.8	64515.1	100786.6	54.5
Case 4	14598.5	1415.63	11672.0	51903.0	79589.91	64.1

TABLE 4. The annual emission amounts result for different case studies.

Objective	Emission amount (g)					
Season	Winter	Spring	Summer	Autumn	Total	Reduction (%)
Case 1	3.0308e+08	2.3290e+08	2.7788e+08	3.8373e+08	1.1976e+09	-
Case 2	2.3230e+08	2.0150e+08	2.5401e+08	3.5944e+08	1.0473e+09	12.5
Case 3	2.1457e+08	1.8897e+08	2.2448e+08	3.3813e+08	9.6615e+08	19.3
Case 4	5.3902e+07	2.4143e+07	1.2944e+08	3.0063e+08	5.0812e+08	57.6

TABLE 5. Comparison between the proposed approach and approaches in [5] and [33].

Index	[5]	[33]	Proposed Approach
Proposed model configuration	CHP, PV, BESS, PHEV without V2G mode	PV, WT, CAES, BESS, TES, PEV without V2G mode, and DRP	Case 4 (PV, WT, CAES, BESS, TES, PEV with V2G mode, and DRP)
Cost reduction (%)	40.0	39.5	64.1
Emission reduction (%)	50.0	36.8	57.6

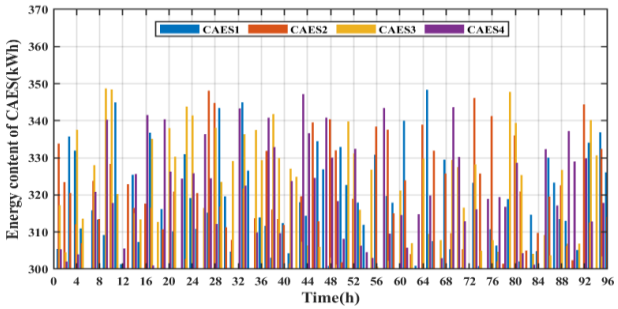

FIGURE 11. Seasonal electrical energy content for CAESs for Case 1.

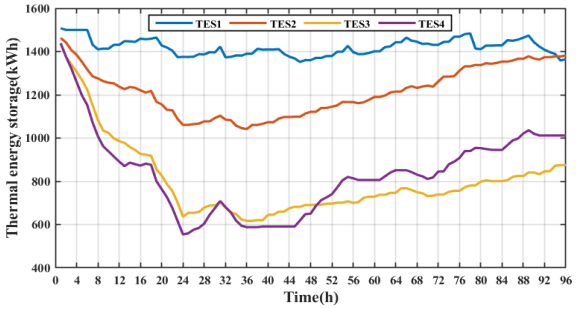

FIGURE 12. Seasonal thermal energy content for TESs for Case 1.

the end-users demand. Though, the parking lot would give each PEV the priority to start charging within its final hours and eventually depart without exceeding the minimum SOC threshold of 75%.

Fig. 18 represents the seasonal charging and discharging power of the different parking lots in the microgrid, denoted by negative and positive values. For instance, during the peak price period elapsed between 4 PM and 8 PM on a typical winter day, parking lots prefer to sell energy stored to the upstream grid. On the other hand, once off-peak periods are experienced and the PEV approaches its final hours in the lot, the lot purchase energy from the upstream grid and adjust the state of the PEV to start charging. One can observe that the presence of the parking lots in the microgrid has dramatically influenced the operation of the EHs. As can be monitored and compared to the base case, the power purchased from the grid, specifically during peak hours, has reduced drastically as a portion of the demands is being fed from the parking lot discharge rather than the grid, see Fig. 17.

B. SUMMARY AND COMPREHENSIVE COMPARISON

In this subsection, a comprehensive comparison regarding the proposed stochastic optimal operation of multi-carrier energy hub-based microgrids is carried out. As previously discussed, the study was conducted on four different case studies.

To evaluate the effectiveness of the proposed stochastic optimal scheduling framework, the total seasonal operation cost and emission amounts are calculated, tabulated, and plotted in Tables 3 and 4, and Fig. 19. For the base case, the total

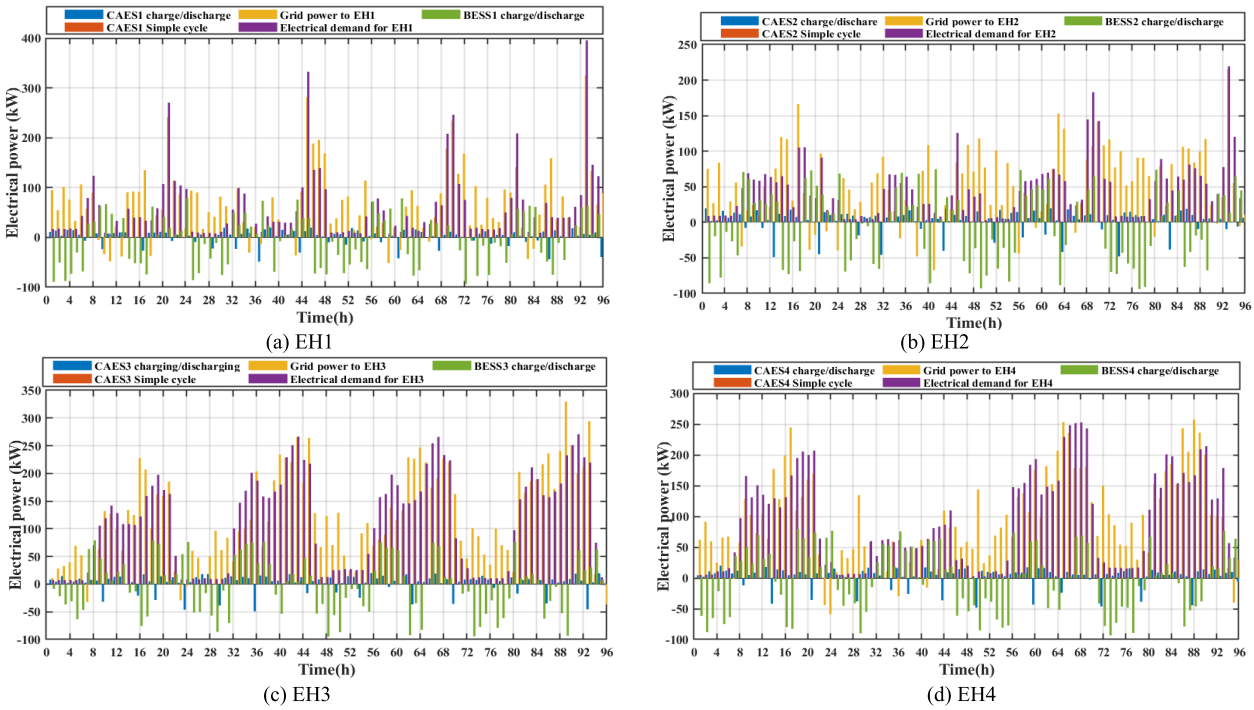

FIGURE 13. Optimal seasonal scheduling results for electrical power flow for Case 2.

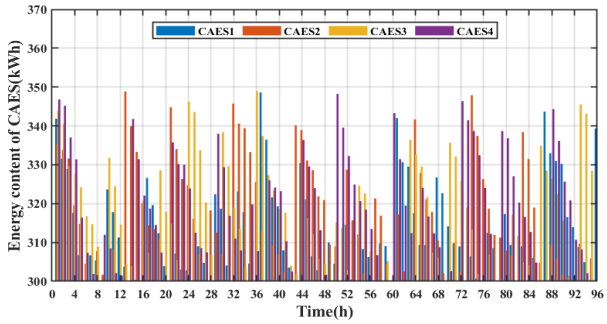

FIGURE 14. Seasonal electrical energy content of CAESs for Case 2.

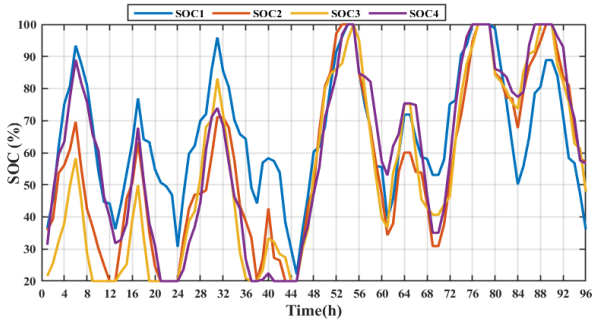

FIGURE 15. Seasonal SOC scheduling of BESSs for Case 2.

operation cost and emissions are calculated as 221,553.2$ and 1.1976e+09 g, respectively, as shown in Tables 3 and 4.

Moreover, the total cost and emissions obtained each season are also displayed in Tables 3 and 4. For Case 2, the total operation cost was reduced by 42.9%, while the total emissions were reduced by 12.5% compared to the base case. Consequently, cost and emissions reductions are obtained each season. This could be justified by BESS supporting the CAES to meet a more significant portion of the demand, leading to less power importing from the utility grid, and more may be sold during peak hours. Another factor that could lead to significant cost and emissions reductions is the DRP. As for Case 3, the employing of the DRP has accounted for 54.5% and 19.3% reductions in the total operation cost and emissions compared to the base case.

Furthermore, the costs and emissions during the various seasons were mitigated compared to the previous two cases (Case 1 and Case 2). For instance, during the wintertime, the cost was evaluated to be 17,383.1$ compared to 22,896.2$ in Case 2. This reduction is reasonably expected as the price-based DRP encourages end users to shift their consumption to the off-peak and low-price hours, resulting in less power purchased from the utility grid during high-price periods. Finally, parking lots have been implemented in Case 4. The total operation cost was significantly reduced by 64.1% and emissions were reduced by 57.6% compared to the base case. Indeed, the total operation cost during the different seasons was reduced. This implies that the charging/discharging scheduling of the PEV contributes to supplying the end-users demands and thus reducing the power imported from the grid. Fig. 19 shows that the total operation cost and emissions are significantly reduced as progressively proceeding from the base case.

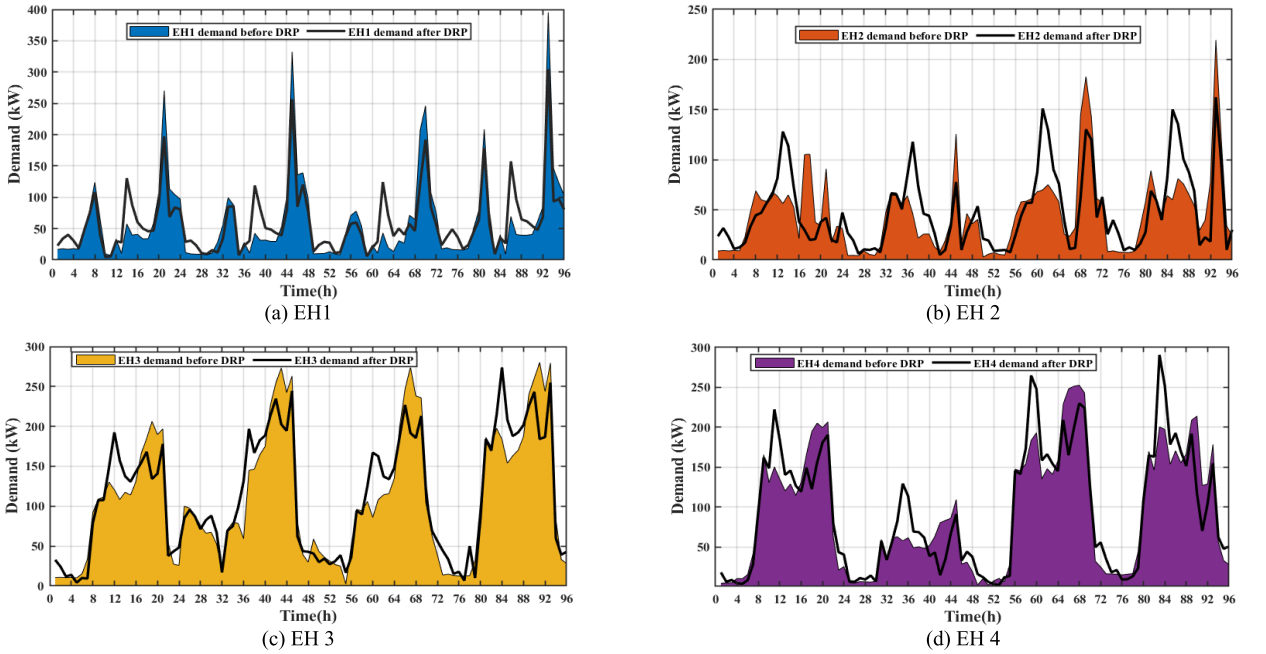

FIGURE 16. Energy hub demands before and after DRP for Case 3.

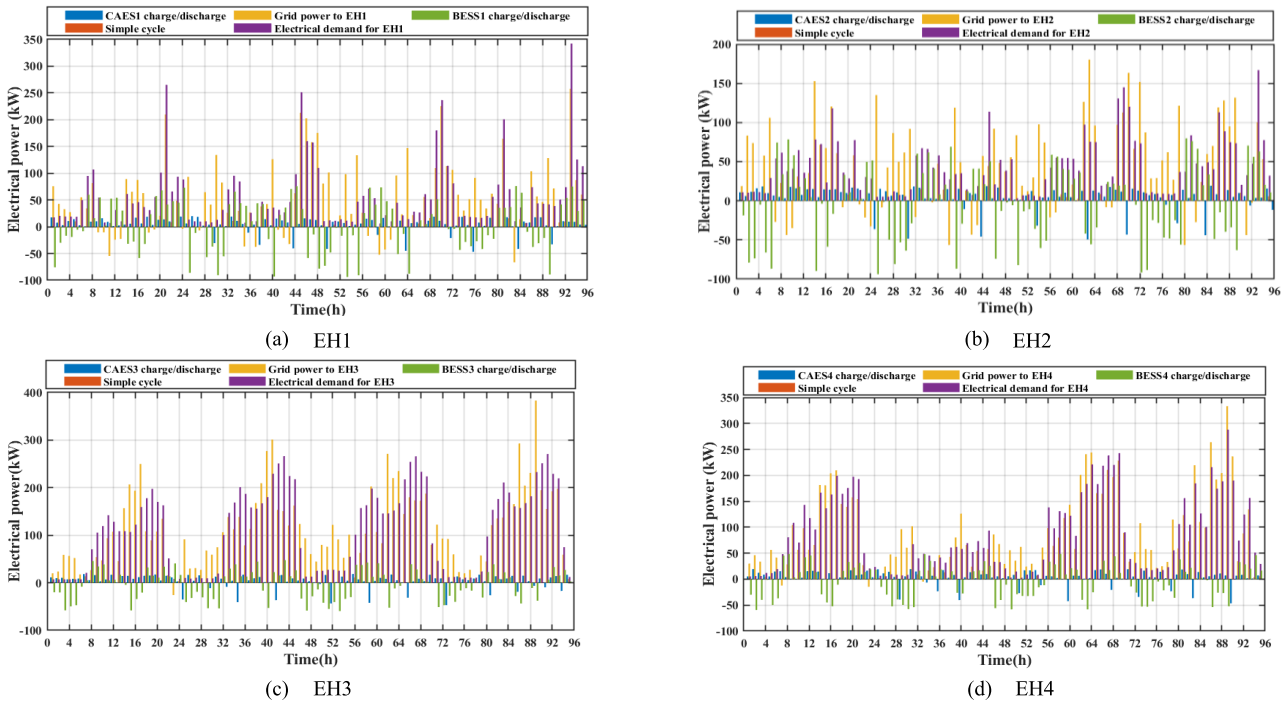

FIGURE 17. Optimal seasonal scheduling results for electrical power flow for Case 4.

To highlight the effectiveness of the proposed approach, a comparison between the proposed models in [5] and [33] has been undertaken in Table 5. For [5], the energy hub model was primarily constructed of CHP, PV, BESS, and PHEV. Accordingly, this approach accounted for 40% and 50.0% reductions in cost and emission, respectively. For [33], the proposed model has completely ignored the V2G capability of the PEVs. As stated earlier, the V2G mode could substantially affect the operation cost and emission by reducing the electric power imported from the grid. On the other hand, the charging of the PEVs could be carried out by the RESs installed. For this case, only 39.5% and 36.8% reductions

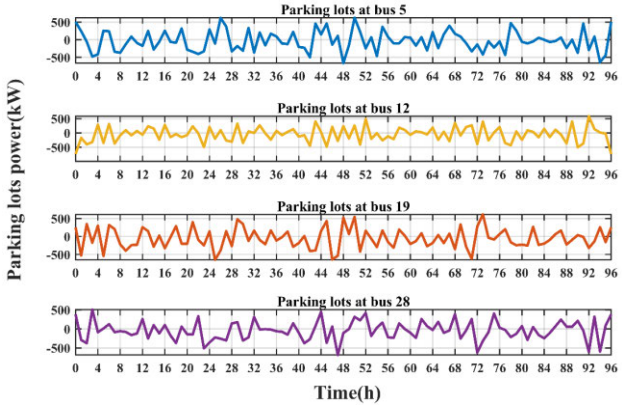

FIGURE 18. Seasonal charging/discharging power for the different parking lots in the system for Case 4.

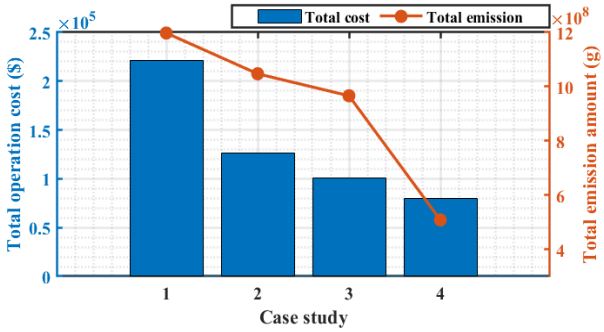

FIGURE 19. Comprehensive comparison between total operation costs and emission amounts for the different case studies considered.

are obtained in the cost and emission in [33], respectively, compared to 64.1% and 57.6% reductions from the proposed work.

IX. CONCLUSION

A stochastic multi-objective optimization framework is proposed in this paper to address the coordinated operation of the CAES, BESS, TES, and PEV along with RES. The model under study has been established to depict four different EHs interconnected into the IEEE-33 at various suggested locations according to the investors' preferences. Uncertainties represented in RES, demands, electricity prices, and driving habits of the PEVs' owners have been considered in the proposed approach. Furthermore, the DRP is implemented to shift the non-obligatory demands to off-peak periods to mitigate the operation cost.

Particularly, this study has considered minimizing two objectives, which are, the operation costs and emission amounts. The MOGWO has been deployed to handle the multi-objective optimization approach and a set of a Pareto front optimal solutions are generated. For decision-making and to select one trade-off optimal solution among the different non-dominated ones, the fuzzy set theory and linear membership function are implemented. The significant findings of this study could be summed up as follows:

- For the first case study, the EH mainly consists of CAES and TES. The CAES undergoes charging, discharging, and simple cycles to satisfy electrical demands. Additionally, the CAES has the capability to satisfy thermal demand. Yet, the thermal generation has a degree of interdependency with the electrical generation as heat could only be generated and efficiently recovered during the discharging cycles. One demerit of relying only on CAES for electrical-thermal demand satisfaction is that the discharge process is associated with a significant amount of CO2, NOx, and SOx which would inevitably deteriorate the emission issues.
- To get around the problem related to the base case, the CAES is coordinated with a BESS. Most of the time during the scheduling horizon, the BESS takes over the satisfaction of the demands as it does not contribute to harmful emissions, leading to a total emission amount reduction of 12.5% compared to the base case. In addition, the generation capacity of each EH has increased which means purchasing less power from the grid and leading to a 42.9% reduction in overall operating cost.
- For the third case, the DRP is applied to shift non-obligatory demands from peak to valley periods, taking into consideration the satisfaction of the comfort preferences level of the consumer. As a result, less power is purchased from the utility grid during high-price periods which is accounted for by a reduction of 54.5% in operation cost. Furthermore, the emission amounts have been mitigated by 19.3%.
- The final case has considered the adoption of the V2G mode of the PEVs which exist at different parking lots located at different buses in the IEEE-33 bus system. The seasonal charging/discharging scheduling of the PEV contributes to supplying the end-users' demands and thus reducing the annual imported power from the grid. As a result, the total operation cost has been mitigated by 64.1%. Moreover, the emission amounts have been dramatically reduced by 57.6%, leading to a greener operation as desired.

ACKNOWLEDGMENT

This article represents the opinions of the authors and does not mean to represent the position or opinions of the American University of Sharjah.

REFERENCES

[1] A. Kazemdehdashti, M. Mohammadi, A. R. Seifi, and M. Rastegar, "Stochastic energy management in multi-carrier residential energy systems," *Energy*, vol. 202, Jul. 2020, Art. no. 117790, doi: 10.1016/j.energy.2020.117790.

[2] G. Abdulnasser, A. Ali, M. F. Shaaban, and E. E. M. Mohamed, "Stochastic multi-objectives optimal scheduling of energy hubs with responsive demands in smart microgrids," *J. Energy Storage*, vol. 55, Nov. 2022, Art. no. 105536, doi: 10.1016/j.est.2022.105536.

[3] A. Bostan, M. S. Nazar, M. Shafie-khah, and J. P. S. Catalão, "Optimal scheduling of distribution systems considering multiple downward energy hubs and demand response programs," *Energy*, vol. 190, Jan. 2020, Art. no. 116349, doi: 10.1016/j.energy.2019.116349.

[4] A. Najafi, H. Falaghi, J. Contreras, and M. Ramezani, "Medium-term energy hub management subject to electricity price and wind uncertainty," *Appl. Energy*, vol. 168, pp. 418–433, Apr. 2016, doi: 10.1016/j.apenergy.2016.01.074.

[5] M. Rayati, A. Sheikhi, and A. M. Ranjbar, "Optimising operational cost of a smart energy hub, the reinforcement learning approach," *Int. J. Parallel, Emergent Distrib. Syst.*, vol. 30, no. 4, pp. 325–341, Jul. 2015, doi: 10.1080/17445760.2014.974600.

[6] M. H. Shams, M. Shahabi, M. Kia, A. Heidari, M. Lotfi, M. Shafie-Khah, and J. P. S. Catalão, "Optimal operation of electrical and thermal resources in microgrids with energy hubs considering uncertainties," *Energy*, vol. 187, Nov. 2019, Art. no. 115949, doi: 10.1016/j.energy.2019.115949.

[7] J. Fang, Q. Zeng, X. Ai, Z. Chen, and J. Wen, "Dynamic optimal energy flow in the integrated natural gas and electrical power systems," *IEEE Trans. Sustain. Energy*, vol. 9, no. 1, pp. 188–198, Jan. 2018, doi: 10.1109/TSTE.2017.2717600.

[8] M. Kazemi, S. Y. Salehpour, F. Shahbaazy, S. Behzadpoor, S. Pirouzi, and S. Jafarpour, "Participation of energy storage-based flexible hubs in day-ahead reserve regulation and energy markets based on a coordinated energy management strategy," *Int. Trans. Electr. Energy Syst.*, vol. 2022, pp. 1–17, Sep. 2022, doi: 10.1155/2022/6481531.

[9] K. Esapour, F. Moazzen, M. Karimi, M. Dabbaghjamanesh, and A. Kavousi-Fard, "A novel energy management framework incorporating multi-carrier energy hub for smart city," *IET Gener., Transmiss. Distrib.*, vol. 17, no. 3, pp. 655–666, Feb. 2023, doi: 10.1049/gtd2.12500.

[10] H. R. Massrur, T. Niknam, and M. Fotuhi-Firuzabad, "Day-ahead energy management framework for a networked gas-heat-electricity microgrid," *IET Gener., Transmiss. Distrib.*, vol. 13, no. 20, pp. 4617–4629, Oct. 2019, doi: 10.1049/iet-gtd.2019.0686.

[11] M. D. Leonard, E. E. Michaelides, and D. N. Michaelides, "Substitution of coal power plants with renewable energy sources—Shift of the power demand and energy storage," *Energy Convers. Manage.*, vol. 164, pp. 27–35, May 2018, doi: 10.1016/j.enconman.2018.02.083.

[12] V. S. Tabar, M. A. Jirdehi, and R. Hemmati, "Sustainable planning of hybrid microgrid towards minimizing environmental pollution, operational cost and frequency fluctuations," *J. Cleaner Prod.*, vol. 203, pp. 1187–1200, Dec. 2018, doi: 10.1016/j.jclepro.2018.05.059.

[13] A. A. Eladl, M. I. El-Afifi, M. A. Saeed, and M. M. El-Saadawi, "Optimal operation of energy hubs integrated with renewable energy sources and storage devices considering CO_2 emissions," *Int. J. Electr. Power Energy Syst.*, vol. 117, May 2020, Art. no. 105719, doi: 10.1016/j.ijepes.2019.105719.

[14] X. Lu, Z. Liu, L. Ma, L. Wang, K. Zhou, and N. Feng, "A robust optimization approach for optimal load dispatch of community energy hub," *Appl. Energy*, vol. 259, Feb. 2020, Art. no. 114195, doi: 10.1016/j.apenergy.2019.114195.

[15] J. Ma, S. Wu, and E. A. Raad, "Renewable source uncertainties effects in multi-carrier microgrids based on an intelligent algorithm," *Energy*, vol. 265, Feb. 2023, Art. no. 126098, doi: 10.1016/j.energy.2022.126098.

[16] C. K. Das, O. Bass, G. Kothapalli, T. S. Mahmoud, and D. Habibi, "Overview of energy storage systems in distribution networks: Placement, sizing, operation, and power quality," *Renew. Sustain. Energy Rev.*, vol. 91, pp. 1205–1230, Aug. 2018, doi: 10.1016/j.rser.2018.03.068.

[17] M. Aldaadi, F. Al-Ismail, A. T. Al-Awami, and A. Muqbel, "A coordinated bidding model for wind plant and compressed air energy storage systems in the energy and ancillary service markets using a distributionally robust optimization approach," *IEEE Access*, vol. 9, pp. 148599–148610, 2021, doi: 10.1109/ACCESS.2021.3123792.

[18] M. Jalili, M. Sedighizadeh, and A. S. Fini, "Optimal operation of the coastal energy hub considering seawater desalination and compressed air energy storage system," *Thermal Sci. Eng. Prog.*, vol. 25, Oct. 2021, Art. no. 101020, doi: 10.1016/j.tsep.2021.101020.

[19] M. Soltani, M. H. Nabat, A. R. Razmi, M. B. Dusseault, and J. Nathwani, "A comparative study between ORC and Kalina based waste heat recovery cycles applied to a green compressed air energy storage (CAES) system," *Energy Convers. Manag.*, vol. 222, Oct. 2020, Art. no. 113203, doi: 10.1016/j.enconman.2020.113203.

[20] A. Kumar, N. K. Meena, A. R. Singh, Y. Deng, X. He, R. C. Bansal, and P. Kumar, "Strategic integration of battery energy storage systems with the provision of distributed ancillary services in active distribution systems," *Appl. Energy*, vol. 253, Nov. 2019, Art. no. 113503, doi: 10.1016/j.apenergy.2019.113503.

[21] W. Zhuo and A. V. Savkin, "Profit maximizing control of a microgrid with renewable generation and BESS based on a battery cycle life model and energy price forecasting," *Energies*, vol. 12, no. 15, p. 2904, Jul. 2019, doi: 10.3390/en12152904.

[22] A. R. Dehghani-Sanij, E. Tharumalingam, M. B. Dusseault, and R. Fraser, "Study of energy storage systems and environmental challenges of batteries," *Renew. Sustain. Energy Rev.*, vol. 104, pp. 192–208, Apr. 2019, doi: 10.1016/j.rser.2019.01.023.

[23] V. V. Thang, Y. Zhang, T. Ha, and S. Liu, "Optimal operation of energy hub in competitive electricity market considering uncertainties," *Int. J. Energy Environ. Eng.*, vol. 9, no. 3, pp. 351–362, Sep. 2018, doi: 10.1007/s40095-018-0274-8.

[24] J. Gao, G. Tian, A. Sorniotti, A. E. Karci, and R. Di Palo, "Review of thermal management of catalytic converters to decrease engine emissions during cold start and warm up," *Appl. Thermal Eng.*, vol. 147, pp. 177–187, Jan. 2019, doi: 10.1016/j.applthermaleng.2018.10.037.

[25] Y. Gan, M. Wang, Z. Lu, and J. Kelly, "Taking into account greenhouse gas emissions of electric vehicles for transportation decarbonization," *Energy Policy*, vol. 155, Aug. 2021, Art. no. 112353, doi: 10.1016/j.enpol.2021.112353.

[26] S. M. Moghaddas-Tafreshi, M. Jafari, S. Mohseni, and S. Kelly, "Optimal operation of an energy hub considering the uncertainty associated with the power consumption of plug-in hybrid electric vehicles using information gap decision theory," *Int. J. Electr. Power Energy Syst.*, vol. 112, pp. 92–108, Nov. 2019, doi: 10.1016/j.ijepes.2019.04.040.

[27] M. Vahid-Ghavidel, M. S. Javadi, M. Gough, S. F. Santos, M. Shafie-Khah, and J. P. S. Catalao, "Demand response programs in multi-energy systems: A review," *Energies*, vol. 13, no. 17, p. 4332, 2020, doi: 10.3390/en13174332.

[28] K. Nainar, J. R. Pillai, and B. Bak-Jensen, "Incentive price-based demand response in active distribution grids," *Appl. Sci.*, vol. 11, no. 1, p. 180, 2021, doi: 10.3390/app11010180.

[29] S. A. Mansouri, A. Ahmarinejad, M. Ansarian, M. S. Javadi, and J. P. S. Catalao, "Stochastic planning and operation of energy hubs considering demand response programs using benders decomposition approach," *Int. J. Electr. Power Energy Syst.*, vol. 120, Sep. 2020, Art. no. 106030, doi: 10.1016/j.ijepes.2020.106030.

[30] S. A. Mansouri, M. S. Javadi, A. Ahmarinejad, E. Nematbakhsh, A. Zare, and J. P. S. Catalão, "A coordinated energy management framework for industrial, residential and commercial energy hubs considering demand response programs," *Sustain. Energy Technol. Assessments*, vol. 47, Oct. 2021, Art. no. 101376, doi: 10.1016/j.seta.2021.101376.

[31] M. Hemmati, M. Abapour, B. Mohammadi-Ivatloo, and A. Anvari-Moghaddam, "Optimal operation of integrated electrical and natural gas networks with a focus on distributed energy hub systems," *Sustainability*, vol. 12, no. 20, p. 8320, 2020, doi: 10.3390/su12208320.

[32] H. Yarmohammadi and H. Abdi, "A comprehensive optimal power and gas flow in multi-carrier energy networks in the presence of energy storage systems considering demand response programs," *Electric Power Syst. Res.*, vol. 214, Jan. 2023, Art. no. 108810, doi: 10.1016/j.epsr.2022.108810.

[33] S. Zeynali, N. Rostami, A. Ahmadian, and A. Elkamel, "Robust multi-objective thermal and electrical energy hub management integrating hybrid battery-compressed air energy storage systems and plug-in-electric-vehicle-based demand response," *J. Energy Storage*, vol. 35, Mar. 2021, Art. no. 102265, doi: 10.1016/j.est.2021.102265.

[34] X. Lu, K. Zhou, S. Yang, and H. Liu, "Multi-objective optimal load dispatch of microgrid with stochastic access of electric vehicles," *J. Cleaner Prod.*, vol. 195, pp. 187–199, Sep. 2018, doi: 10.1016/j.jclepro.2018.05.190.

[35] M. Mohiti, H. Monsef, and H. Lesani, "A decentralized robust model for coordinated operation of smart distribution network and electric vehicle aggregators," *Int. J. Electr. Power Energy Syst.*, vol. 104, pp. 853–867, Jan. 2019, doi: 10.1016/j.ijepes.2018.07.054.

[36] A. Ali, K. Mahmoud, and M. Lehtonen, "Optimization of photovoltaic and wind generation systems for autonomous microgrids with PEV-parking lots," *IEEE Syst. J.*, vol. 16, no. 2, pp. 3260–3271, Jun. 2022, doi: 10.1109/JSYST.2021.3097256.

[37] M. Tasdighi, H. Ghasemi, and A. Rahimi-Kian, "Residential microgrid scheduling based on smart meters data and temperature dependent thermal load modeling," *IEEE Trans. Smart Grid*, vol. 5, no. 1, pp. 349–357, Jan. 2014, doi: 10.1109/TSG.2013.2261829.

[38] R. Li and S. SaeidNahaei, "Optimal operation of energy hubs integrated with electric vehicles, load management, combined heat and power unit and renewable energy sources," *J. Energy Storage*, vol. 48, Apr. 2022, Art. no. 103822, doi: 10.1016/j.est.2021.103822.
[39] G. Alva, Y. Lin, and G. Fang, "An overview of thermal energy storage systems," *Energy*, vol. 144, pp. 341–378, Feb. 2018, doi: 10.1016/j.energy.2017.12.037.
[40] A. Nayak, A. Maulik, and D. Das, "An integrated optimal operating strategy for a grid-connected AC microgrid under load and renewable generation uncertainty considering demand response," *Sustain. Energy Technol. Assessments*, vol. 45, Jun. 2021, Art. no. 101169, doi: 10.1016/j.seta.2021.101169.
[41] A. J. Nebro, J. J. Durillo, and C. A. C. Coello, "Analysis of leader selection strategies in a multi-objective particle swarm optimizer," in *Proc. IEEE Congr. Evol. Comput.*, Jun. 2013, pp. 3153–3160, doi: 10.1109/CEC.2013.6557955.
[42] S. Mirjalili, S. Saremi, S. M. Mirjalili, and L. D. S. Coelho, "Multi-objective grey wolf optimizer: A novel algorithm for multi-criterion optimization," *Exp. Syst. Appl.*, vol. 47, pp. 106–119, Apr. 2016, doi: 10.1016/j.eswa.2015.10.039.
[43] B. Khorshid-Ghazani, H. Seyedi, B. Mohammadi-ivatloo, K. Zare, and S. Shargh, "Reconfiguration of distribution networks considering coordination of the protective devices," *IET Gener., Transmiss. Distrib.*, vol. 11, no. 1, pp. 82–92, Jan. 2017, doi: 10.1049/iet-gtd.2016.0539.
[44] S. Gupta, A. Maulik, D. Das, and A. Singh, "Coordinated stochastic optimal energy management of grid-connected microgrids considering demand response, plug-in hybrid electric vehicles, and smart transformers," *Renew. Sustain. Energy Rev.*, vol. 155, Mar. 2022, Art. no. 111861, doi: 10.1016/j.rser.2021.111861.
[45] A. Ghanbari, H. Karimi, and S. Jadid, "Optimal planning and operation of multi-carrier networked microgrids considering multi-energy hubs in distribution networks," *Energy*, vol. 204, Aug. 2020, Art. no. 117936, doi: 10.1016/j.energy.2020.117936.
[46] *Flatirons M2 Daily Data*. Accessed: Jan. 23, 2023. [Online]. Available: https://midcdmz.nrel.gov/apps/day.pl?NWTC
[47] P. Kayal and C. K. Chanda, "Optimal mix of solar and wind distributed generations considering performance improvement of electrical distribution network," *Renew. Energy*, vol. 75, pp. 173–186, Mar. 2015, doi: 10.1016/j.renene.2014.10.003.

ABDELFATAH ALI received the B.Sc. and M.Sc. degrees in electrical engineering from Aswan University, Aswan, Egypt, in 2009 and 2013, respectively, and the Ph.D. degree from the Doctoral School of Electrical Engineering, Budapest University of Technology and Economics, Budapest, Hungary, in 2020. Since 2010, he has been an Assistant Lecturer with the Faculty of Engineering, South Valley University (SVU), Qena, Egypt. In 2020, he was appointed as an Assistant Professor with SVU, where he is on leave. He is currently a Postdoctoral Research Fellow with the American University of Sharjah, Sharjah, United Arab Emirates. In 2022, he was a Guest Editor of *Energies* (MDPI) journal. He has been recognized as one of the best reviewers of the IEEE TRANSACTIONS ON SUSTAINABLE ENERGY. In 2023, he was a Guest Editor of a Special Issues on Grid Efficiency in *Frontiers in Smart Grids*. His research interests include smart grids, the integration of renewable energy resources, electric vehicles, and operation, optimization, and the control of distribution systems.

MOSTAFA F. SHAABAN (Senior Member, IEEE) received the B.Sc. and M.Sc. degrees in electrical engineering from Ain Shams University, Cairo, Egypt, in 2004 and 2008, respectively, and the Ph.D. degree in electrical engineering from the University of Waterloo, Waterloo, ON, Canada, in 2014. Currently, he is an Associate Professor with the Department of Electrical Engineering, American University of Sharjah, Sharjah, United Arab Emirates, and an Adjunct Professor with the University of Waterloo. He has several publications in international journals and conferences and serves as an Associate Editor for *IET Smart Grid* and a reviewer for several refereed journals. His research interests include smart grid, renewable DG, distribution system planning, electric vehicles, storage systems, and bulk power system reliability.

ESSAM E. M. MOHAMED was born in Qena, Egypt, in 1974. He received the B.Sc. and M.Sc. degrees in electrical power and machines engineering from the Faculty of Energy Engineering, Aswan University, Aswan, Egypt, in 1997 and 2003, respectively, and the Ph.D. degree in electrical engineering from The University of Sheffield, Sheffield, U.K., in 2011.

In 1999, he joined the Department of Electrical Engineering, Faculty of Energy Engineering, Aswan University. Since 2013, he has been with the Department of Electrical Engineering, Faculty of Engineering, South Valley University, Qena. His research interests include power electronics, electrical machines design and control, electric drives, and renewable energy systems. He is the Founder and a Manager of the South Valley University IEEE Student Branch.

GHADA ABDULNASSER was born in Qena, Egypt, in 1997. She received the B.Sc. degree in electrical power and machines engineering from South Valley University, Qena, in 2020. In 2021, she joined the Department of Electrical Engineering, Faculty of Engineering, and is currently a Teaching Assistant. Her research interests include electrical power systems, energy hubs, and electric vehicles.